T.R.

GEBZE TECHNICAL UNIVERSITY

GRADUATE SCHOOL OF NATURAL AND APPLIED SCIENCES

DEVELOPMENT OF Bi_2O_3 BASED-ELECTROLYTES FOR LOW-TEMPERATURE SOFC APPLICATIONS

YAVUZ SELİM AYHAN

A THESIS SUBMITTED FOR DEGREE OF

MASTER OF SCIENCE

DEPARTMENT OF MATERIALS SCIENCE AND ENGINEERING

GEBZE

2018

T.R.

GEBZE TECHNICAL UNIVERSITY

GRADUATE SCHOOL OF NATURAL AND APPLIED SCIENCES

DEVELOPMENT OF Bi_2O_3 BASED-ELECTROLYTES FOR LOW-TEMPERATURE SOFC APPLICATIONS

YAVUZ SELIM AYHAN

A THESIS SUBMITTED FOR THE DEGREE OF

MASTER OF SCIENCE

DEPARTMENT OF MATERIALS SCIENCE AND ENGINEERING

THESIS SUPERVISOR

ASST. PROF. DR. ALIGUL BUYUKAKSOY

GEBZE

2018

T.C.
GEBZE TEKNİK ÜNİVERSİTESİ
FEN BİLİMLERİ ENSTİTÜSÜ

DÜŞÜK SICAKLIKTA ÇALIŞAN KATI OKSİT YAKIT HÜCRELERİ İÇİN Bi_2O_3 TABANLI ELEKTROLİTLERİN GELİŞTİRİLMESİ

YAVUZ SELİM AYHAN
YÜKSEK LİSANS TEZİ
MALZEME BİLİMİ VE MÜHENDİSLİĞİ ANABİLİM DALI

DANIŞMANI
DR. ÖĞR. ÜYESİ ALİGÜL BÜYÜKAKSOY

GEBZE
2018

GEBZE TEKNİK ÜNİVERSİTESİ	YÜKSEK LİSANS JÜRİ ONAY FORMU

GTÜ Fen Bilimleri Enstitüsü Yönetim Kurulu'nun 05/12/2018 tarih ve 2018/59 sayılı kararıyla oluşturulan jüri tarafından 17/12/2018 tarihinde tez savunma sınavı yapılan Yavuz Selim AYHAN'ın tez çalışması Malzeme Bilimi ve Mühendisliği Anabilim Dalında YÜKSEK LİSANS tezi olarak kabul edilmiştir.

JÜRİ

ÜYE (TEZ DANIŞMANI)	: Dr. Öğr. Üyesi Aligül BÜYÜKAKSOY
ÜYE	: Prof. Dr. Ahmet Yavuz ORAL
ÜYE	: Prof. Dr. Cleva W. Ow-Yang

ONAY

Gebze Teknik Üniversitesi Fen Bilimleri Enstitüsü Yönetim Kurulu'nun

...../...../..... tarih ve ...../..... sayılı kararı.

SUMMARY

Despite obvious advantages of solid oxide fuel cells (SOFCs), they have some problems that need to be addressed for their commercialization. The major issue is that high operating temperatures (~800 °C) cause performance loss due to microstructural and chemical degradation with time.

In order to overcome the performance loss, lowering the operating temperatures of SOFCs down to below 650 °C is the straightforward approach. Doped bismuth oxide ceramics are quite promising for low temperature SOFC electrolyte applications due to their extremely high ionic conductivity. However, the stability of its fast-ionic conductor phase (cubic-δ) at this targeted operating temperature is questionable.

In this work, the effects of the fabrication conditions of 28 mol% Y_2O_3 doped Bi_2O_3 (YDB) on the phase and electrical conductivity stability was investigated. It was shown that the sintering temperature greatly affects the phase and electrical conductivity stability. For example, YDB ceramics sintered at 800 °C exhibited a fast, exponential-type conductivity decay with a concomitant cubic to rhombohedral phase transformation upon a 100-hour exposure to 650 °C. Conversely, all the YDB ceramics sintered at higher temperatures (900-1100 °C) experienced a slower, linear conductivity decay under the same conditions, but with no observable phase transformation. This difference was connected to the higher amount of metastable cubic-δ phase present in YDB sintered at 800 °C than those sintered at higher temperatures.

Practically, it was suggested that for SOFC applications, the conventional approach of lowering the sintering temperature to reduce the manufacturing costs would result in poor stability in YDB electrolytes.

Keywords: Bi_2O_3 Based Electrolytes, Yttria Doped Bismuth Oxide, Solid Oxide Fuel Cell, Impedance Spectroscopy, Long-Term Stability.

ÖZET

Katı oksit yakıt hücreleri (KOYH) bilinen avantajlarına rağmen, piyasaya sürülebilmeleri için halen bazı problemlerinin çözülmesi gerekmektedir. En büyük sorun bu cihazların yüksek sıcaklıklarda (~800 °C) çalışmalarıdır. Bu sıcaklıklarda KOYH bileşenleri zamanla mikroyapısal ve kimyasal bozunmalara uğrar ve bu sebeple performans kaybı meydana gelir.

Performans kaybını önlemek için KOYH sisteminin çalışma sıcaklığını düşürmek 650 °C'nin altına düşürmek en temel yaklaşım olarak karşımıza çıkmaktadır. Yüksek iyonik iletkenlikleri sebebiyle katkılanmış bizmut oksit seramikleri düşük sıcaklıkta çalışan KOYH elektrolitleri için gayet uygun malzemelerdir. Fakat, hedeflenen çalışma sıcaklıklarında yüksek iyonik iletkenlik gösteren kübik-δ fazının kararlılığı tartışmalıdır.

Bu çalışmada, molce %28 Y_2O_3 ile katkılanmış Bi_2O_3 (YKB)'nin üretim şartlarının faz ve elektriksel iletkenlik kararlılığı üzerindeki etkisi araştırılmıştır. Sinterleme sıcaklığının faz ve elektriksel iletkenlik kararlılığı üzerinde büyük bir etkisi olduğu görülmüştür. Örneğin, 800 °C'de sinterlenmiş YKB seramikleri, 650 °C'de 100 saat ısıl işleme tabi tutulduklarında elektriksel iletkenliklerinde eksponansiyel tipte, hızlı bir düşüş göstermişlerdir. Bu düşüşe kübik fazdan rombohedral faza dönüşüm eşlik etmiştir. Diğer yandan, yüksek sıcaklıkta (900-1100 °C) sinterlenmiş YKB seramikleri aynı şartlar altında doğrusal tipte ve daha yavaş bir iletkenlik kaybı göstermişlerdir. Fakat, bu seramiklerde bir faz dönüşümü saptanamamıştır. Aradaki bu farkın, 800 °C'de sinterlenmiş YKB seramiklerinde daha yüksek sıcaklıklarda sinterlenmiş numunelere göre daha yüksek miktarda yarı-kararlı kübik-δ fazı bulunması olduğu öne sürülmüştür.

Uygulama açısından bakıldığında, üretim masraflarını düşürmek için geleneksel yaklaşım olan sinterleme sıcaklığının düşürülmesinin, YKB elektrolitlerinde düşük kararlılığa sebep olduğu tespit edilmiştir.

Anahtar Kelimeler: Bi_2O_3 Tabanlı Elektrolitler, İtriya Katkılanmış Bizmut Oksit, Katı Oksit Yakıt Hücresi, Empedans Spektroskopisi, Uzun Dönem Stabilizasyonu.

ACKNOWLEDGEMENTS

I would like to express my deep and sincere gratitude to my supervisor, Dr. Aligul Buyukaksoy, who not only shared his profound scientific knowledge with me but also taught me great lessons of life. His support, suggestions and encouragement gave me the drive and will to complete this work.

I wish to express my warm and sincere thanks to my colleagues for their motivational help and collaboration in some parts of the work.

I am really grateful to members of my big family– Mustafa, Sibel, Aysenur, Semra, Hamdi and Telat, my fiancé – Mirac and my lovely grandfather – Ali Ulviks for their love and support.

I am really thankful that this project is funded by TUBITAK (Project no: 217M031).

TABLE of CONTENTS

LIST of ABBREVIATIONS and ACRONYMS

Abbreviations and Acronyms		**Explanations**
δ- Bi_2O_3	:	Bismuth Oxide with Fluorite Structure
ASR	:	Area Specific Resistance
Bi_2O_3	:	Bismuth Oxide
DTA	:	Differential Thermo Gravimetric Analysis
EIS	:	Electrochemical Impedans Spectroscopy
KOYH	:	Katı Oksit Yakıt Hücresi
PSA	:	Particle Size Distribution
SEM	:	Scanning Electron Microscopy
SOFC	:	Solid Oxide Fuel Cell
XRD	:	X-ray Diffraction
Y_2O_3	:	Yttrium Oxide
YDB	:	Yttria Doped Bismuth Oxide
YSZ	:	Yttria Stabilized Zirconia

LIST of FIGURES

LIST of TABLES

1. INTRODUCTION

1.1. The Energy Problem

Energy consumption of the world rises due to increasing population, developing technology and the pursuit of a higher life standard. To meet this need of energy, combustion of fossil fuels is still preferred predominantly. However, this way of producing energy causes air pollution due to high CO_2 emissions [1]. In addition, fossil fuels are not renewable. Therefore, researchers have been developing new methods to generate electricity efficiently and with no/less harmful gas emissions, such as fuel cells. Basically, fuel cells are electrochemical devices that convert chemical energy into electrical energy by electro-chemical reactions. The two well-known types of fuel cells are proton exchange membrane fuel cells (PEMFCs) and solid oxide fuel cells (SOFCs).

Solid oxide fuel cells (SOFCs) work with high efficiency (>80%) and realize energy conversion at high temperatures which provide fuel flexibility, i.e; hydrocarbon or hydrogen gas can be used as fuel. In the case of hydrocarbon use, the high energy conversion efficiency enables slow depletion of resources and low CO_2 emissions. On the other hand, the case of hydrogen use allows for zero carbonaceous gas release and provides a system which can be integrated into renewable energy systems.

1.2. The Working Principle of Solid Oxide Fuel Cells

A solid oxide fuel cell (SOFC) is based on an oxygen ion conducting, dense (hence gas-tight) ceramic membrane (solid electrolyte) which is placed between two porous electrodes, namely cathode and anode as schematically shown in Figure 1.

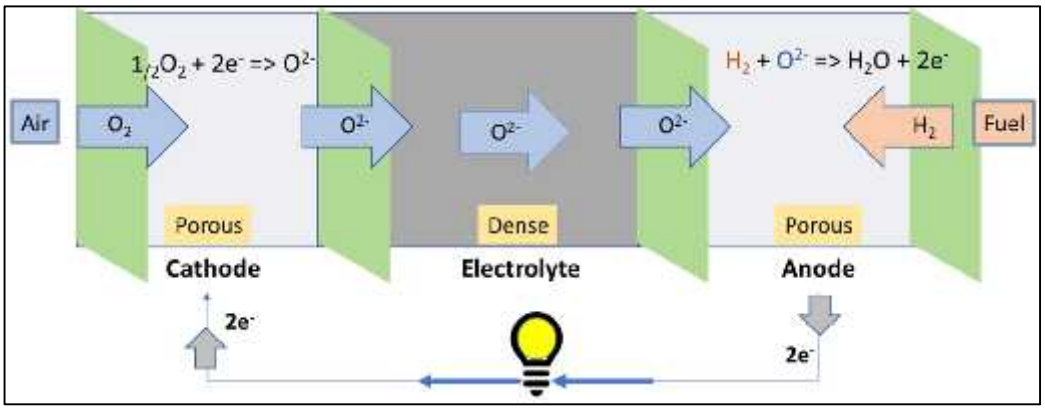

Figure 1.1: Schematic representation of working principle of solid oxide fuel cells.

When fuel and air gases are purged from the anode and cathode sides respectively at high temperatures, an open circuit voltage is generated, obeying the Nernst equation. (Equation 1.1)

$$E = E_0 + \frac{RT}{nF}\left(\frac{P_{H_2} P_{O_2}^{\frac{1}{2}}}{P_{H_2O}}\right) \tag{1.1}$$

Here E is the generated open circuit potential, E_0 is the standard potential, R is the ideal gas constant, n is the number of electrons, F is the Faraday constant and P_i is the partial pressure of the relevant gas species (i.e. H_2, O_2 or H_2O).

To convert the obtained voltage into useful electrical work, the circuit is closed and current is drawn. The electrochemical phenomena that take place during current flow is schematically explained in Figure 1.1. The oxygen gas at the cathode side is reduced to oxide ions by combining with electrons via Equation 1.2. The oxide ions are transported through the ionic conductor electrolyte to the anode side.

$$\frac{1}{2}O_2 + 2e^- = O^{-2} \tag{1.2}$$

The oxide ions now at the fuel rich porous anode combine with the hydrogen gas to produce water vapor and electrons (Equation 1.3). This way the circuit is completed.

$$H_2 + O^{-2} = 2e^- + H_2O \tag{1.3}$$

During current flow, the voltage of the SOFC system drops due to three types of kinetic losses in the cell:

- Activation losses

  Voltage drop associated with the rates of the electrochemical reactions at the electrodes.

- Ohmic losses

  Losses caused by the resistance to ionic transport within the electrolyte.

- Mass-transfer losses

  Also named as “concentration polarization”, mass transfer losses occur as a result of the limited transported reactant gases to the electrochemical reaction sites at the electrodes. Figure 1.2 shows the voltage losses in a typical I-V curve obtained from a SOFC [2].

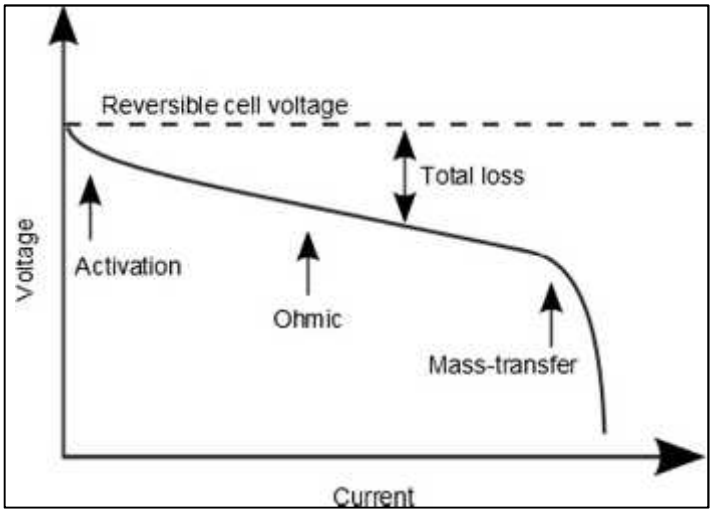

Figure 1.2: V-I curve to show voltage losses in a fuel cell.

1.3. Materials Selection For Solid Oxide Fuel Cells

- Electrolyte

  As mentioned earlier, the electrolyte must exhibit high ionic conductivity and no electronic conductivity to achieve open circuit potentials close to the theoretically

predicted values from Equation 1.1 and to achieve low ohmic electrolyte losses. The oxygen ion conductivity is a function of the oxygen diffusion coefficient and thus is a thermally activated process, as described in the Nernst-Einstein relation in Equation 1.4. Here, σ is conductivity, T is temperature, z is the valance, e is the electronic charge, c_i is the number of charged particles (concentration) per unit volume, u is the jump distance, β_i is the particle mobility, k is the boltzman constant, D_i is the diffusion coefficient, ΔH_m is the enthalpy change.

$$\sigma_i T = z_i e c_i u_i T = (z_i e)^2 c_i B_i T = \frac{(z_i e)^2 c_i}{k} D_i = \frac{(z_i e)^2 c_i}{k} D_{i,0} \exp\frac{-\Delta H_m}{kT} \quad (1.4)$$

This expression can be reduced to a simpler form by collecting all the pre-exponential parameters together into a single factor A:

$$\sigma T = A \exp(-EA / kT) \quad (1.5),$$

where σ is oxygen ion conductivity, T is temperature, A is a pre-exponential term, E is the activation energy, and k is the Boltzmann constant.

Figure 1.3 shows the temperature dependence of the electrical conductivities of various types of electrolyte materials, in air [3]. It is interesting to note that the most widely used SOFC electrolyte material - yttria stabilised zirconia (YSZ) with the cubic fluorite structure does not exhibit the highest electrical conductivity at lower temperatures (≤650 °C). However, it exhibits remarkable phase stability under both reducing and oxidizing conditions with an ideal oxygen transfer number (t_{O2}=1)' rendering this material so attractive.

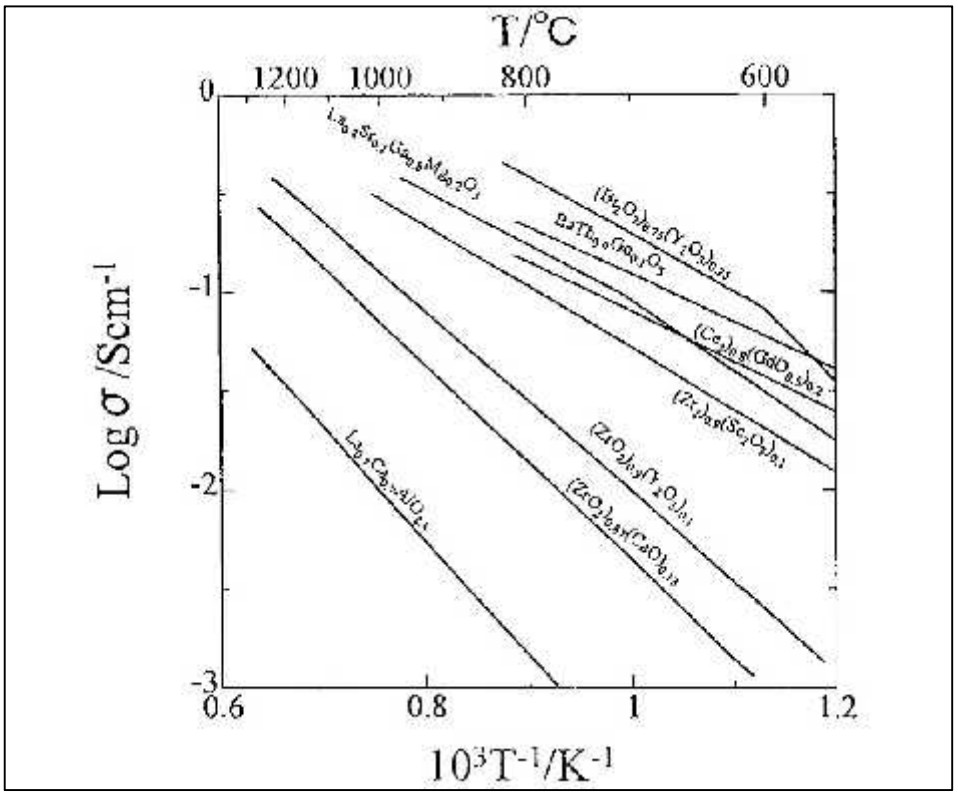

Figure 1.3: Comparison of conductivity of various solid electrolytes.

Among these materials, it is evident that $(Bi_2O_3)_{0,75}(Y_2O_3)_{0,25}$ (YDB) – another fluorite structured material - exhibits the highest electrical conductivity of 0.16 S/cm at 700 ºC [4]. At lower temperatures, such as 500 ºC, ionic conductivity of YDB which is $1.3x10^{-2}$ is ca. two orders of magnitude higher than the commonly used YSZ ($4.6x10^{-4}$) [4]. This roughly corresponds to more than a 200 °C reduction in the SOFC operating temperature without any compromise from the electrolyte ohmic losses, if the YSZ electrolytes could be replaced by YDB. This significant difference between bismuth oxide and other cubic fluorite phase electrolytes such as ZrO_2, CeO_2 originates from the presence of additional 25 mol% oxygen vacancies resulting from the 3^+ oxidation state of Bi as opposed to the 4^+ oxidation states of Ce and Zr. Figure 1.4b provides a schematic representation of the cubic fluorite structures of ceria [4] and bismuth oxide [5].

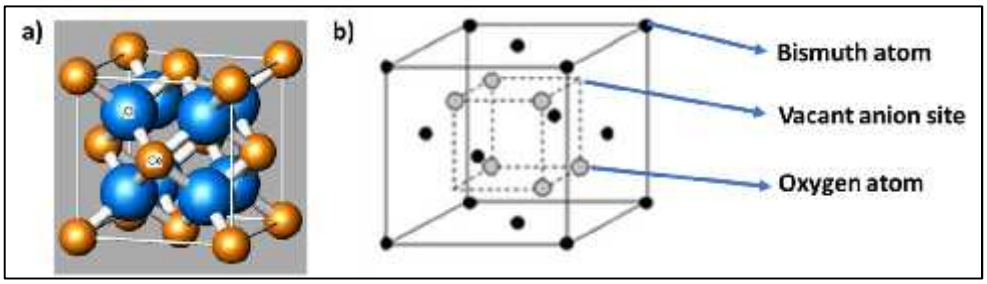

Figure 1.4: Cubic fluorite structure of a) ceria and b) bismuth oxide.

However, YDB exhibits poor chemical stability under reducing conditions, i.e., Bi_2O_3 reduces to metallic Bi under hydrogen flow from the anode side at 600 ºC [6]. This problem can be circumvented by adopting a bilayer electrolyte design, which consists of a thin, dense YSZ protective layer onto the anode side of the YDB electrolyte. But even then, the issue of the stability of the fluorite phase stability of the YDB electrolyte must be addressed, since electrical conductivity decay takes place upon long-term operation at 500 and 650 °C, due to ordering and cubic to hexagonal phase transformations at the respective temperatures [7]-[10].

- Cathode

In the cathode layer, reduction of oxygen gas into oxygen ions takes place. This requires that i) oxygen gas molecules are adsorbed onto the cathode material, ii) oxygen gas molecules are combined with electrons to produce oxygen ions and iii) oxygen ions are delivered to the electrolyte. To maintain these three requirements, sufficient porosity for oxygen gas delivery, electronic conductivity and oxygen ion conductivity must be provided within the cathode layer. This is usually realized by forming a porous composite material that consists of an elecrocatalytically active phase (that is also an electronic conductor) and an ionic conductor phase. The electrocatalytic material is Sr doped $LaMnO_3$ (LSM) and the ionic conductor phase is YSZ in most cases [11], [12].

- Anode

In a similar fashion, for effective fuel oxidation, a porous composite material that consists of an electrocatalytic (also an electronic conductor) material and an ionic conductor is used in the anode side. The most best performing material has been the Ni-YSZ composites [13], [14]. For an effective anode works efficiently in

the SOFC system needs some properties – porosity, ionic conductivity and electronic conductivity. Well-known materials to provide these properties are Nickel-yttria stabilized zirconia (YSZ).

2. LITERATURE REVIEW AND SCOPE OF THIS WORK

2.1. Problems of The SOFC Technology

Despite their obvious advantages, SOFCs have some issues that need to be addressed before they are commercialized. SOFCs have been known as high temperature fuel cells since they were invented. The reason was that the YSZ electrolyte shows acceptable ionic conductivity only at the 800-1000 °C temperature range [15]. However, these high operating temperatures constitute an extremely harsh environment for the SOFC components, causing performance loss with time [16]. For example, dopant segregation takes place at the surface of the cathode materials such as (La,Sr)MnO (LSM) and (La,Sr)CoO (LSC) upon long term operation [17]. In addition, the nickel particles within the Ni-yttria stabilized zirconia (YSZ) composite anode undergoes coarsening at these temperatures, yielding a loss of electrochemically active zones, more specifically triple phase boundaries (TPBs) – the intersection of the Ni, YSZ and gas phases [18]. Moreover, ferritic steels – cost effective candidates for cathode side interconnect materials - oxidize and become unusable above 650 °C.

In order to overcome the issues mentioned in the previous section, operating SOFCs at lower temperatures (≤650 °C) is the most straightforward approach. In addition to the prevention of chemical and microstructural degradation in the electrode materials, it also avoids long startup times, allows the use of ferritic steels as interconnects and drops the cost of production in the system [19]. However, lowering the operating temperature of SOFCs, results in higher electrolyte resistances. Reducing the electrolyte thickness down to 1-10 μm range has proven ineffective by itself to make up for the exponentially enhanced ohmic electrolyte resistances. Even if a thin electrolyte approach is adopted, the SOFC design becomes an electrode-supported one, which has significant drawbacks, such as; intolerance to redox cycles [20], [21] and high-temperature electrode processing yielding coarse microstructures and thus high electrode polarization resistances [22].

In conclusion, the use of electrolyte materials with ionic conductivities much higher than that of YSZ appears inevitable to lower the operating temperature of SOFCs without significant performance loss.

2.2. Literature Survey on Bismuth Oxide-based Ceramics

Bi_2O_3 has four polymorphs, namely, α, β, γ, δ phases [23], the latter being the highly conductive fluorite type structure, which exists above 730 °C [24]. The cubic fluorite phase (δ) of Bi_2O_3 exhibits a higher oxygen ion conductivity in comparison to their polymorphs because i) it has 25% of the oxygen sites vacant and ii) Bi^{+3} cations are highly polarizable allowing facile oxygen ion transport [25].

However, to be used in SOFC applications, bismuth oxide must remain in its high conductivity phase δ-cubic at the temperature range between room temperature and the operating conditions. To ensure this stabilization, bismuth oxide has been doped with rare-earth oxides such as Y_2O_3 [26], Gd_2O_3 [27], Er_2O_3 [28] and etc.

Although initial studies suggested that stabilization of the cubic phase down to room temperature was achieved by this approach [29], further investigations proved that the observed δ-cubic phases were only metastable, and prolonged exposure to targeted SOFC operating temperatures, e.g., 650 °C still resulted in phase transformation from cubic to rhombohedral [29]. This phase transformation was concomitant with a conductivity decay [30]. Another type of structural degradation that also causes conductivity loss is anion ordering [31]. Several studies showed that upon prolonged exposure to 500 °C, rare earth doped bismuth oxide underwent a significant conductivity decay which was not accompanied by a phase change observable by X-ray diffraction [10], [32], [33]. Neutron diffraction studies revealed later that anion sublattice ordering, which causes a decrease in the number of available vacant sites of an oxygen ion were the origin of the conductivity decay [31].

In order to avoid conductivity decay that these two mechanisms cause in doped Bi_2O_3 electrolytes, a few studies were reported in the literature. For example, N. Jiang and Wachsman suggested doubly or triply doped bismuth oxides. They reported that and Dy_2O_3 and Ho_2O_3 doped Bi_2O_3 exhibits the lowest rate of degradation among them due to the largest cation radius of the material [9]. Moreover, K.Z. Fung et al. suggest that adding of ZrO2 into doped bismuth oxide systems is a useful way to avoid phase transformation [34].

2.3. Scope of This Work

Despite the intense efforts to understand the origins of the long-term instability of the electrical conductivity bismuth oxide-based SOFC electrolytes and to avoid this phenomena [9], [10], [24], [30], [35]-[38], very few studies focus on the fabrication of these ceramics [39], [40]. Moreover, no studies exist in the literature on the effects of the fabrication conditions on the long-term stability of the electrical conductivity of bismuth oxide-based ceramics. In fact, heat treatment at a wide range of temperatures may be required to achieve dense bismuth oxide ceramics depending on the powder characteristics. This, in turn, may influence the amount of metastable δ-phase [41] which may have a significant impact on the phase transformation kinetics.

In the present work, the synthesis of YDB powder via Pechini method and the production of dense YDB ceramics by sintering disc-shaped pellets at 800-1100 °C is presented. The effect of sintering temperature on the density, microstructure, crystal structure, electrical conductivity and the stability of these properties upon long-term exposure to a low SOFC operating temperature of 650 °C are determined. The results of this study clearly show that the temperature at which the YDB ceramics are fabricated is an important parameter that determines the electrical conductivity degradation mechanism for the first time in the literature.

3. EXPERIMENTAL

3.1. Powder Synthesis

To fabricate the $Bi_{1.44}Y_{0.56}O_3$ electrolyte ceramics first, fine, well-dispersed powders are synthesized via the Pechini method. This method involves the dissolution of nitrate salts of the constituent cations in water and the polymerization of the solution by using the appropriate chelating agents. Pechini method allows the dispersion of two or more cations homogenously within the polymer network, allowing the achievement of the complex oxide compounds at relatively low temperatures [42].

Yttrium(III) nitrate hexa-hydrate (Alfa Aesar, 99.8% trace metals basis) and bismuth (III) nitrate penta-hydrate (Alfa Aesar, ACS reagent ≥98.0%) were mixed in stoichiometric amounts, corresponding to 1.67 gram of yttrium (III) nitrate hexahydrate and 5.5 grams of bismuth (III) nitrate pentahydrate. The two compounds were dissolved in a mixture of nitric acid (6 g) and distilled water (6 g) by stirring at a speed of 400 rpm. In this process, we observed that the nitrate salts are not soluble in distilled water, as reported in the literature [43], therefore nitric acid, which serves both as a solvent and a polymerizing agent, was added. After the solution becomes clear, ethylene glycol (14 g) which also acts as a polymerizing agent was added and the resultant solution was stirred for 30 minutes without heat. The mixture was then heated up to 200 ^oC and stirred for another 24 hours in order to allow for the decomposition of organics. The obtained dried gel was calcined at different temperatures; 300, 450, 600, 700 ^oC for 4 hours to achieve the desired fluorite phase. Figure 3.1 shows the flowchart of the powder synthesis procedure.

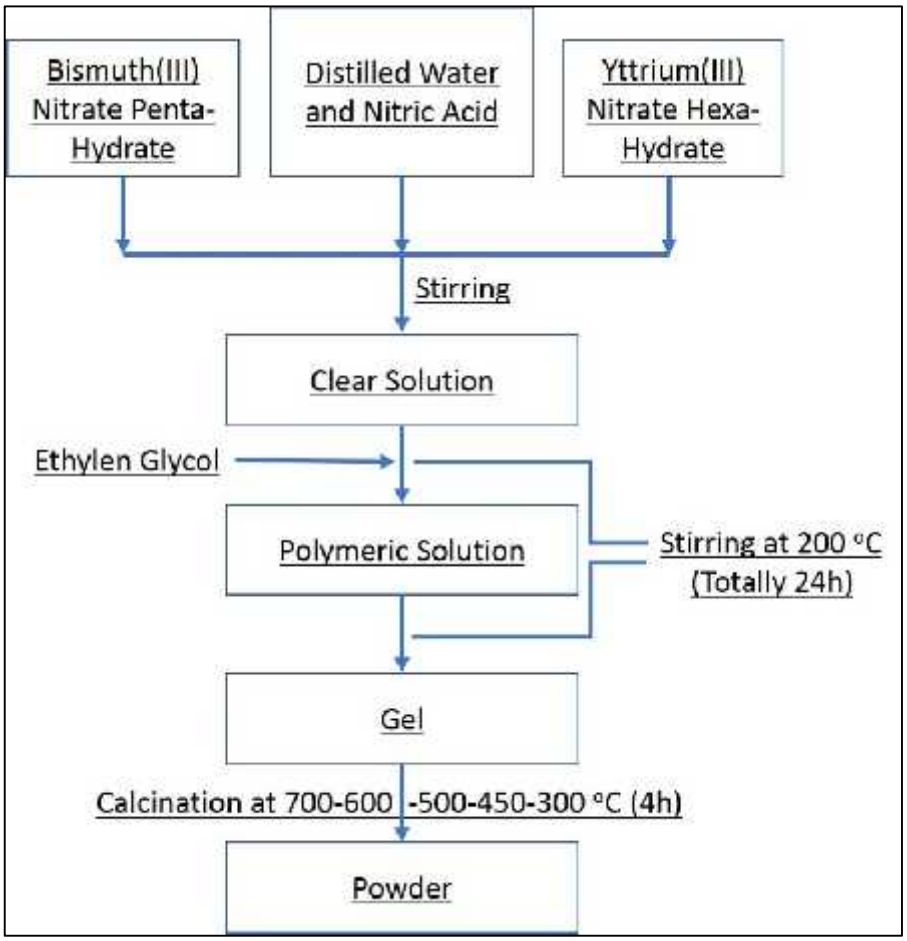

Figure 3.1. Flowchart showing the steps followed to form YDB powders via Pechini method.

For easy sintering of powders into ceramic electrolytes, the synthesized powder was ball milled in ethanol for 24 hours at 140 rpm to obtain sub-micron sized, well-dispersed powders with soft/no agglomerates. The milling was performed in a suspension containing 6.5 grams of powder with 75 grams of ethanol and 100 grams of ZrO_2 milling media, all in a plastic bottle. The milled powder was dried in an oven at 120 °C for 3 hours to make the powder ready for consolidation. In order to find out the crystallite size of calcined and milled YDB particles, Scherer equation was used for the calculation;

$$D_p = \frac{K.\lambda}{\beta cos\theta} \qquad (2.1)$$

where D_p is the average crystallite size (nm), K is Scherer constant related to crystallite shape, and it varies from 0.68 to 2.08 (K = 0.94 for spherical crystallites with cubic

symmetry), λ is the X-ray wavelength in nanometer (nm), β is full width at half maximum (FWHM) of the XRD peak, θ is the X-ray peak position (half of 2θ).

3.2. Powder Consolidation and Sintering

For the assessment of sinterability, phase and microstructure evolution, electrical conductivity and long-term stability, the synthesized powders were consolidated into disc-shaped pellets by die pressing prior to sintering for the sake of robustness. However, for the development of SOFCs with high performance, thin YDB ceramics (e.g., thickness ≤ 200μm) must be fabricated. For that purpose, the synthesized YDB powders were also shaped into thin sheets by tape casting (Figure 3.2).

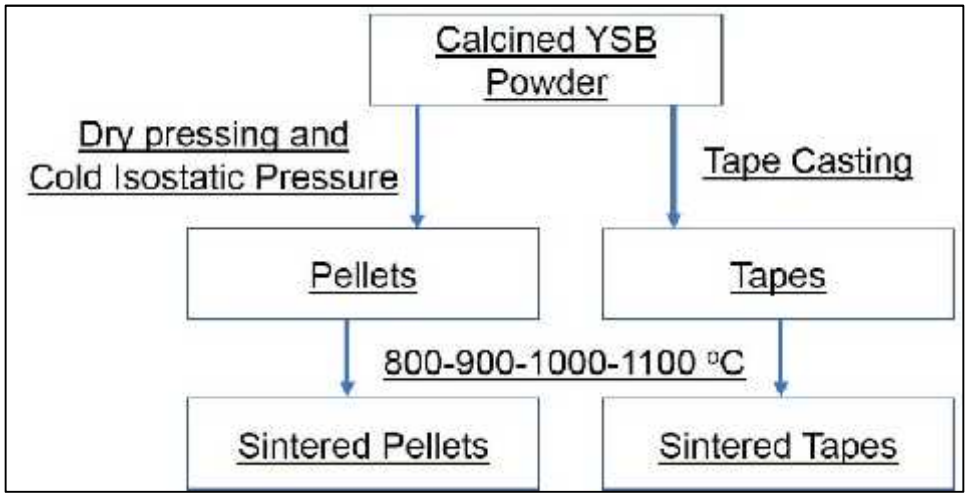

Figure 3.2: The flow chart from YDB powder to the sintered pellets and tapes.

For die pressing; a die with a 10 mm diameter was used. 0.70 grams YDB powder per pellet was pressed with and 0.25 ton force to obtain a preliminary consolidation. For efficient powder packing, the die pressed green bodies were subjected to a cold isostatic pressure of 200 MPa. The obtained pellets were sintered at 800, 900, 1000 or 1100 °C for 6 hours in air to obtain dense ceramic bodies.

For tape casting, YDB powders must be dispersed in a liquid which should possess the right rheology, green-strength and plasticity. The preparation of a tape casting slurry starts with solvent preparation. 7.80 grams of ethyl alcohol and 16.89 grams of toluene were mixed with 2 grams of Poly vinyl butyral (PVB) and 1 gram of dibutyl phthalate (DOP), which serve as binder and plasticizer respectively. After

stirring for 3-5 hours, 5 grams of YDB powder, 10 grams of the binder mixture and 30 milling balls were put into a plastic container (150 ml) and ball milled for 24 hours. Then, the resultant slurry with the dispersed powders was stirred with a magnetic stirrer at room temperature to evaporate the solvents and obtain a more viscous slurry suitable for tape casting. The YDB slurry was cast into tapes using a doctor blade onto Mylar sheets (obtained from Polinas, Turkey). The as-cast tapes were dried at room temperature, in ambient atmosphere, resulting in flexible tapes (Figure 3.3) with a thickness of ca. 300 μm. The sintering of tapes was performed at 1000 °C for 6 hours using a heating plan that involves a burnout step at 350 °C (Figure 3.4).

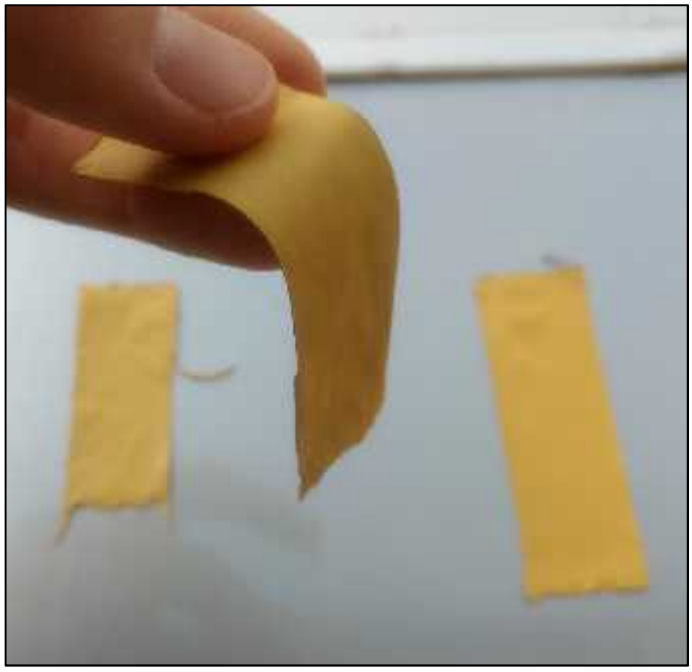

Figure 3.3: Photograph of a YDB tape after drying for 12 hours.

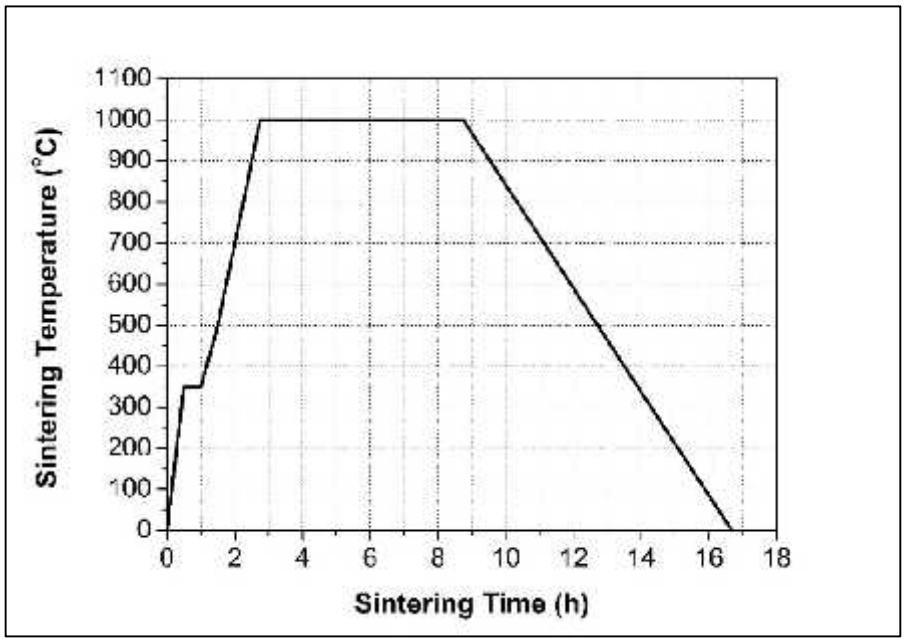

Figure 3.4: Heating regime for sintering YDB tapes.

3.3. Characterization Methods

3.3.1. Crystal Structure Determination

The crystal structure of the fabricated bismuth oxide-based ceramics is crucial to obtain the desired electrical properties. For example, bismuth oxide-based ceramics exhibit their highest ionic conductivity in the cubic fluorite (δ) phase. Therefore, it is crucial to determine the crystal structure of the synthesized powders, the sintered YDB ceramics before and after long-term exposure to the targeted operating temperatures of 650 °C. The crystal structure determination was carried out by the X-ray diffraction (XRD) technique using D/MAX-2200, RIGAKU -Germany with Cu Kα radiation.

3.3.2. Particle Size Analysis

Particle size distrubition (PSD) is the method for using to analysize particle size of powders via laser diffraction. YDB powder into ethanol after ball milling for 24 hours was analysized by particle size analyzer (Malvern MASTERSIZER 2000 - England).

3.3.3. Density Measurements

The density of the sintered ceramic pellets was measured by dividing the mass measured by a laboratory scale (Precisa, Switzerland) by the sample volume calculated from the dimensions measured by a compass. To determine the sample dimensions, six measurements were performed and their average was used to calculate the volume. To determine the density of a YDB ceramic sintered at a certain temperature, the average of density of five samples was calculated. In addition, density measurements were performed via the Archimedes method to test the validity of the results obtained from the geometrical density measurements. The relative density values were determined by dividing the measured density to the theoretical density of 8.1 g/cm^3 obtained from the PDF card number: 01-077-0375.

3.3.4. Microstructural Analysis

The microstructural evolution of the YDB ceramics during sintering and upon long-term annealing at 650 °C, scanning electron microscopy (SEM) analyses were performed (XL30S-FEI-USA). For the SEM analyses of the sintered ceramics, the pellets were broken into two pieces and the fracture surfaces were analyzed. To provide electron collection and hence avoid charging effects, the samples were sputtered with gold.

3.3.5. Electrical Characterization

Electrochemical impedance spectroscopy (EIS) is useful technique to distinguish electrolyte and contact resistances. In order to measure the electrochemical impedance, usually a sinusoidal potential is applied to the electrochemical cell and the resulting sinusoidal current along with the phase shift is measured. The applied sinusoidal potential and the resultant sinusoidal voltage are represented by Equations 2.2 and 2.3.

$$E_t = E_0 \sin(\omega t) \tag{2.2}$$

$$I_t = I_0 \sin(\omega t + \varphi) \tag{2.3}$$

Here, where E_t is the observed potential at time t, E_0 is the input voltage, I_t is the resultant current at time t, I_0 is the maximum amplitude of the response current, ω is the frequency (in Hz) times 2π and φ is phase angle between input and output. In order to calculate the impedance of the system, following Ohm's Law, the potential is divided by current, which can be represented in the form of Equation 2.4;

$$Z = \frac{E_t}{I_t} = \frac{E_0 \sin(\omega t)}{I_0 \sin(\omega t + \varphi)} = Z_0 \frac{\sin(\omega t)}{\sin(\omega t + \varphi)} \quad (2.4)$$

The impedance is now defined in terms of an impedance magnitude, Z_o and a phase shift φ. Using Euler's relationship, this can also be represented as;

$$Z(\omega) = \frac{E}{I} = Z_0 exp(j\varphi) = Z_0(cos\varphi + jsin\varphi) \quad (2.5)$$

where *j* is the imaginary unit. The expression given in Equation 2.5 is an impedance function with real ($Z_{real} = Z_o cos\varphi$) and imaginary ($Z_{imaginary} = Z_o sin\varphi$) components and can be represented in the following form, called the Nyquist plot (Figure 3.5).

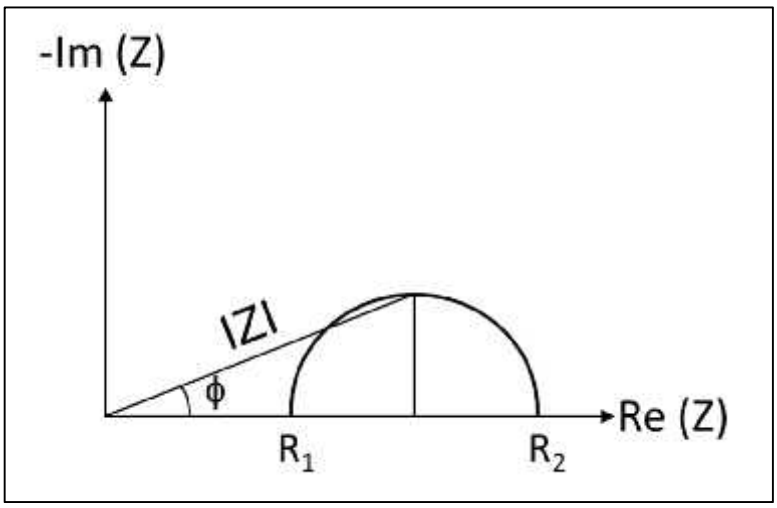

Figure 3.5: A typical EIS data.

In this graph, the first horizontal intercept (R_1) refers to a resistance where there is no phase shift, i.e., no capacitive phenomenon.

The electrochemical impedance spectroscopy measurements were performed on symmetrical half-cells with silver electrodes formed by brush-painting an in-house Ag ink on both sides of the YDB ceramics. Ag lead wires were bonded using a high-

temperature glue (Cerastil, Panacol, Germany). Figure 3.6 shows the photographs of symmetrical half-cell based on pelletized and tape-cast YDB ceramics. The EIS measurements of YDB ceramics sintered at 800-1100 °C were performed at 350-650 °C in a Protherm (PTF 12/50/250, Turkey) tube furnace in stagnant air using a Biologic-SP150 potentiostat/galvanostat/EIS analyzer.

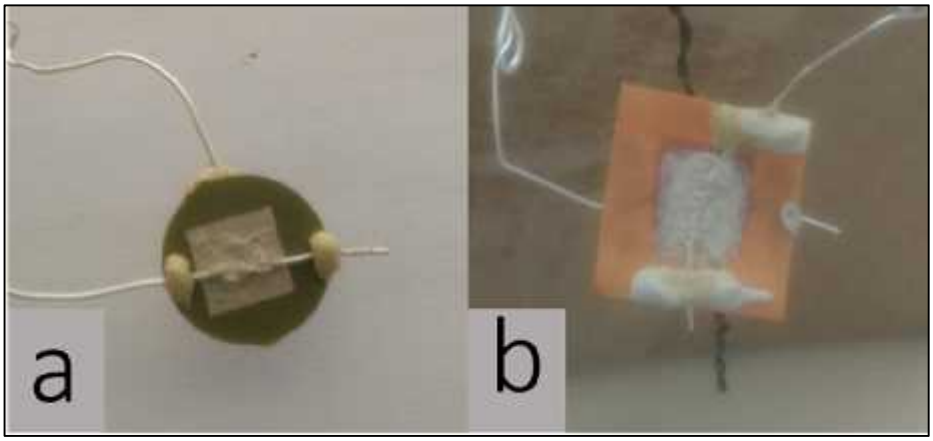

Figure 3.6: Photograph of symmetrical half-cells based on YDB ceramics in a) pellet and b) tape forms with silver electrodes and wires.

4. RESULTS AND DISCUSSION

4.1. Powder Synthesis and Characterization

Bi_2O_3 has generally been doped with 25 mol% Y_2O_3 to stabilize the cubic-δ structure with the high electrical conductivity [10], [30], [33], [40]. In this work, similarly, 28 mol% Y_2O_3 was added to Bi_2O_3 to ensure that the composition stabilize the cubic phase.

The crystal structure of the yttria doped bismuth oxide (YDB) powders synthesized by a Pechini method are determined by X-ray diffraction. Figure 4.1 shows the XRD patterns obtained from powders calcined at the 300-700 °C temperature range. Evidently, no separate Y_2O_3 phases are formed upon calcination at the selected temperature range. On the other hand, only calcination at 700 °C allows the formation of the cubic-δ phase (PDF: 01-077-0375), while at lower calcination temperatures peaks corresponding to the tetragonal phase (PDF: 00-054-1159) is observed. Therefore, to obtain dense YDB ceramics with the cubic-δ structure, YDB powders synthesized by calcining at 700 °C is used.

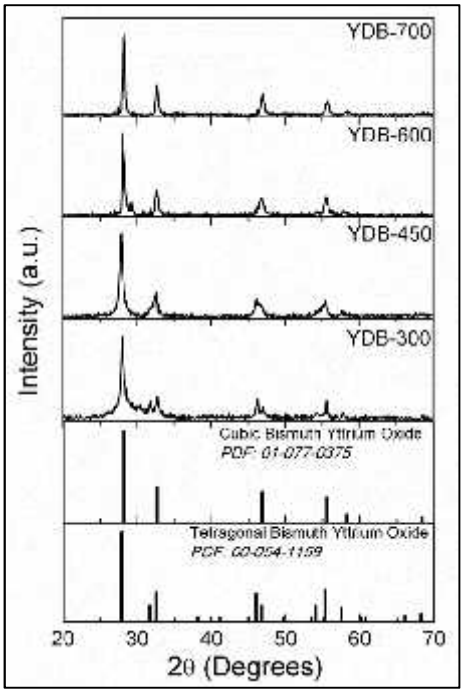

Figure 4.1: X-ray diffraction (XRD) patterns of YDB calcined powders.

Since a dense structure with no interconnected porosity is strictly needed in electrolyte materials for SOFC applications, YDB powders with high sinterability, i.e., small average particle size with a monodisperse distribution, are required. The particle size analysis conducted on YDB powders calcined at 700 °C reveals a poly-disperse particle size distribution with an average particle size of ca. 14 µm (Figure 4.2a), suggesting that a ball milling procedure is required. Figure 4.2b shows that after ball milling the YDB powders in ethanol using zirconia milling media, an average particle size of ca. 200 nm with a monodisperse distribution is achieved.

Homogenously distributed powder with a spherical shape would lessen the risk of coarsening during sintering. To further investigate the powder characteristics, scanning electron microscopy (SEM) analyses were performed on powders after ball milling. Figure 4.3 shows that ball milling leads to a sub-micron, homogenously distributed powders. However, along with spherical ones, a few acicular particles are also observed (Figure 4.3).

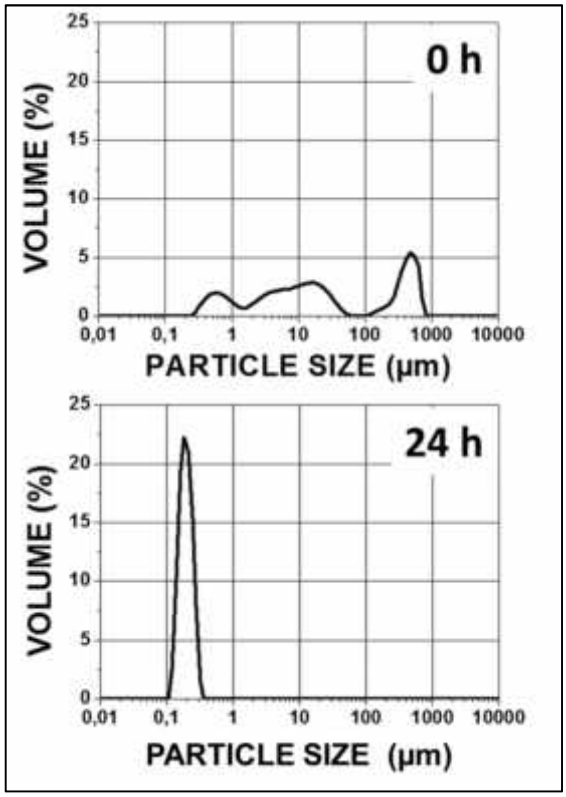

Figure 4.2: Particle size distribution of YDB powder after ball milling.

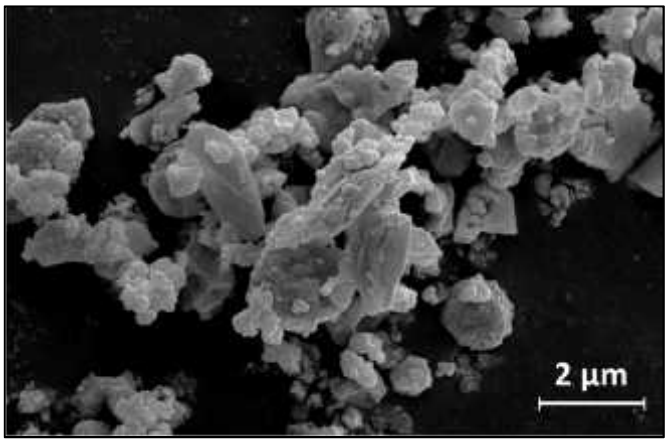

Figure 4.3: A representative scanning electron microscopy image of the YDB powder synthesized by a Pechini method after calcination at 700 °C for 4 hours and 24 hours of ball milling.

The crystallite size of the calcined powders were determined using the Scherrer equation (2.1). The determined average crystallite size of 20 nm is even lower than that reported in literature, (i.e., 85 nm in [44]). This difference likely originates from the lower heat treatment temperature used in the present study (i.e., 700 °C) than that reported in the literature (i.e., 800 °C in [44]).

4.2. Densification and Microstructure of YDB Ceramics

YDB powders were sintered at 800-1100 °C for 6 hours after consolidation into i) disc shaped pellets by die pressing and ii) two dimentional tapes by tape casting. Figures 4.4 and 4.5 show the pellets and tapes before and after sintering at various temperatures. In Figure 4.4 the pellet before sintering (a) has a yellowish color and other (b), (c), (d) and (e) exhibit different colors than (a) and each other by the effect of sintering temperatures at 800, 900, 1000 and 1100 °C; respectively. The big color difference seems that between (b) and other sintered samples. The difference may be caused by scattering due to relatively porous structure of the sample sintered at 800 °C. Figure 4.5 exhibits the before and after sintering of the tape sintered at 1000 °C for 6 hours.

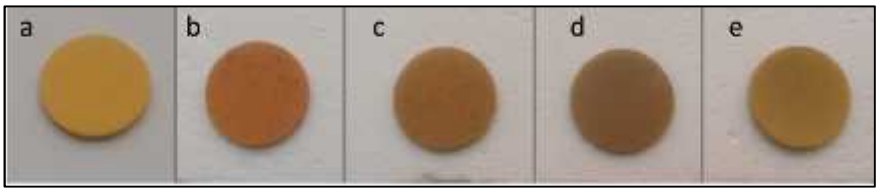

Figure 4.4: Image of the pellets before sintering (a) and after sintering for 6 hours at 800 °C (b), 900 °C (c), 1000 °C (d), 1100 °C (e).

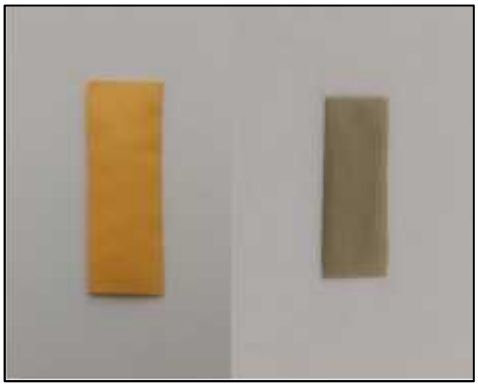

Figure 4.5: Image of the tapes before (left) and after (right) sintering at 1000 °C for 6 hours.

XRD analyses were carried out also after the sintering of consolidated powders to determine the crystal structure of the YDB in the dense ceramic form prior to its testing for SOFC electrolyte application. Figure 4.6 shows that cubic-δ phase (PDF: 01-077-0375) is obtained regardless the sintering temperature (800-1100 °C). According to thereports in the literature, a wide range of heat treatment temperatures allow the formation of pure cubic-δ phase in YDB ceramics [10], [30], [39], [40]. For example; N. Jiang et al [10] obtained cubic-δ phase in 25YDB ceramics sintered in air at 900 °C for 16 hours and Q. Zhen et al. [40] sintered 25YDB samples at 550, 600 and 670 for different length of time and obtained pure phase cubic after 75 minutes.

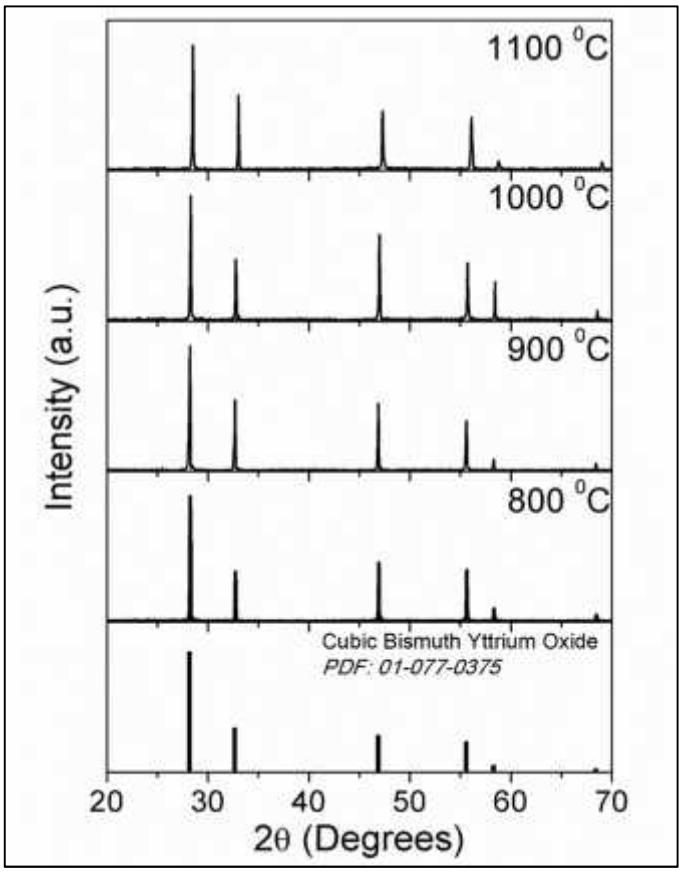

Figure 4.6: The X-ray diffraction patterns of as-sintered YDB pellets at 800-1100 °C.

The effect of sintering temperature on the lattice parameter calculated from the (400) XRD peaks of the cubic-δ phase shown in Figure 4.6 is provided in Table 4.1. In the literature, Jiang et al. [33] determined the lattice parameter of 25YDB as 5.495 Å and Tan et al. [45] calculated the lattice parameter of 30 mol% Y_2O_3 doped Bi_2O_3 (30YDB) as 5.478 Å. The lattice parameters are found to lie in the 5.441-5.481 Å range in the present study for 28YDB ceramics sintered at 800-1100 °C, which appear to be in agreement with the literature [33], [45].

According to Table 4.1, a general decrease in lattice parameter with increasing sintering temperature is observed. This decrease may be caused by the dopant Y^{3+} preferring different lattice positions at different sintering temperatures. For example; at high sintering temperatures, Y^{+3} with the smaller cation radius (0.90 Å [46]) may be replacing the larger Bi^{+3} cation (1.03 Å [46] substitutionally, represented as Y_{Bi}^{x} in the Kröger-Vink notation in Equation 3.1. This would cause an overall decrease in the lattice parameter.

$$Y_2O_3 \rightarrow 2Y_{Bi}^{x} + 3O_o^{x} \quad (3.1)$$

Table 4.1: The change in lattice parameter of YDB ceramics versus sintering temperatures at 800-1100 °C.

Sintering Temperatures (°C)	Lattice parameter (A°)
800	5.473
900	5.445
1000	5.463
1100	5.426

Alternatively, at lower temperatures Y^{+3} may be preferring the interstitials (denoted as $Y_i^{\cdots}$) within the Bi_2O_3 lattice, which would be compensated by the generation of bismuth vacancies (V_{Bi}^{lll}) as shown in Equation 3.2, which would not cause such a dramatic decrease in the lattice parameter.

$$Y_2O_3 \rightarrow 2Y_i^{\cdots} + 2V_{Bi}^{lll} + 3O_o^x \qquad (3.2)$$

The effect of sintering temperature on the microstructure of the YDB ceramics were determined by SEM analysis. Fracture surface image of the YDB pellets in Figures 4.7a (and its inset) indicate that sintering at 800 °C for 6 hours in stagnant air yields a microstructure with interconnected porosity. On the other hand, sintering pellets at 900-1100 °C yields denser microstructures with several isolated pores (Figures 4.7b-d).

The SEM image of a single layer YDB tape sintered at 1000 °C for 6 hours reveals a thickness of ca. 65 microns (Figure 4.8a) with a microstructure similar to that observed in pellets sintered at 1000 °C for the same duration (Figure 4.8b). For an SOFC with a YDB electrolyte supported design, the optimum thickness which would yield the highest mechanical strength and the lowest area specific ohmic resistance must be determined. The obtained thickness of 65 microns (Figure 4.8a) is evidently too thin for such an application. The investigations on finding the desired thickness by fabricating tapes of variable thicknesses by setting up Doctor Blade height during tape casting are currently underway.

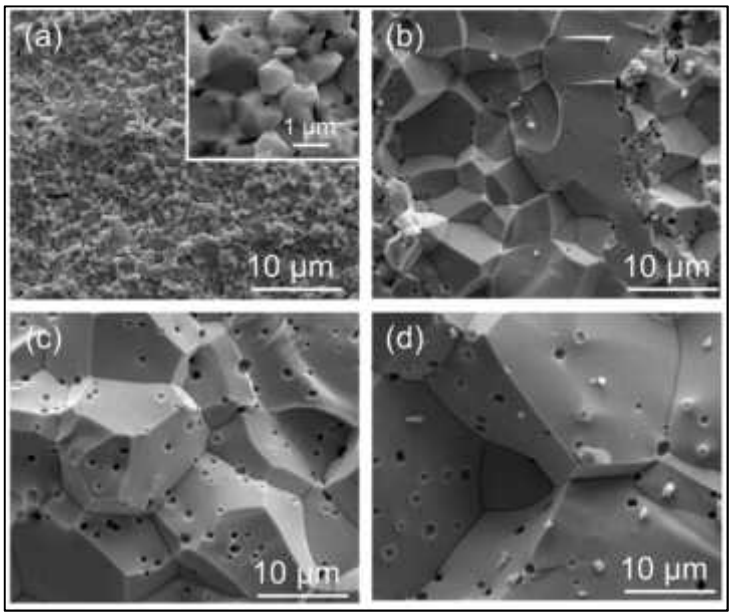

Figure 4.7: Cross-section scanning electron microscopy images of YDB pellets sintered at a) 800, b) 900, c) 1000, d) 1100 °C.

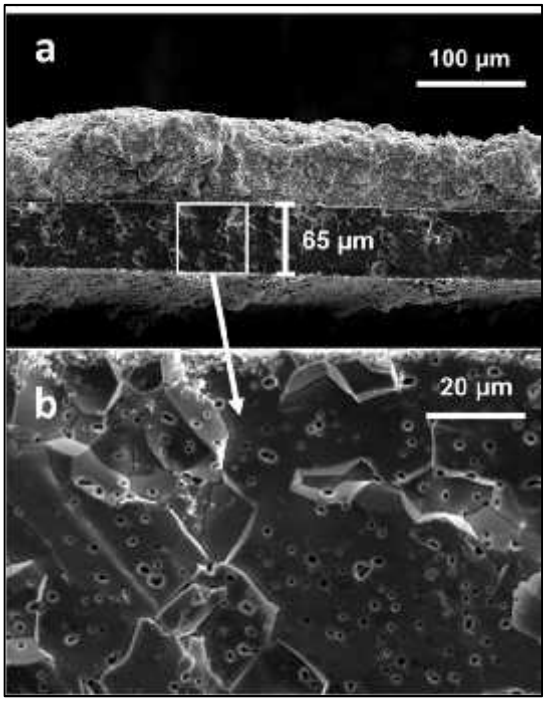

Figure 4.8: Cross-section scanning electron microscopy image of YDB tape sintered at 1000 °C shows the thickness of YDB tape.

Increasing temperature in sintering conditions may lead to increasing effect upon grain size and pore size in the structure, which is related to coarsening mechanism being more active along with desification (Figure 4.7a-d).

The relative density and the average grain size of YDB ceramics were determined by geometry/weight measurements and SEM image analysis via intercept method. Figure 4.9a shows that sintering the YDB ceramics at 800 °C results in a ca. 83% relative density, which must contain interconnected porosity, in agreement with the SEM images (Figure 4.7a). At higher sintering temperatures, relative densities exceeding 90% (corresponding to closed porosity) is obtained (Figure 4.9a).

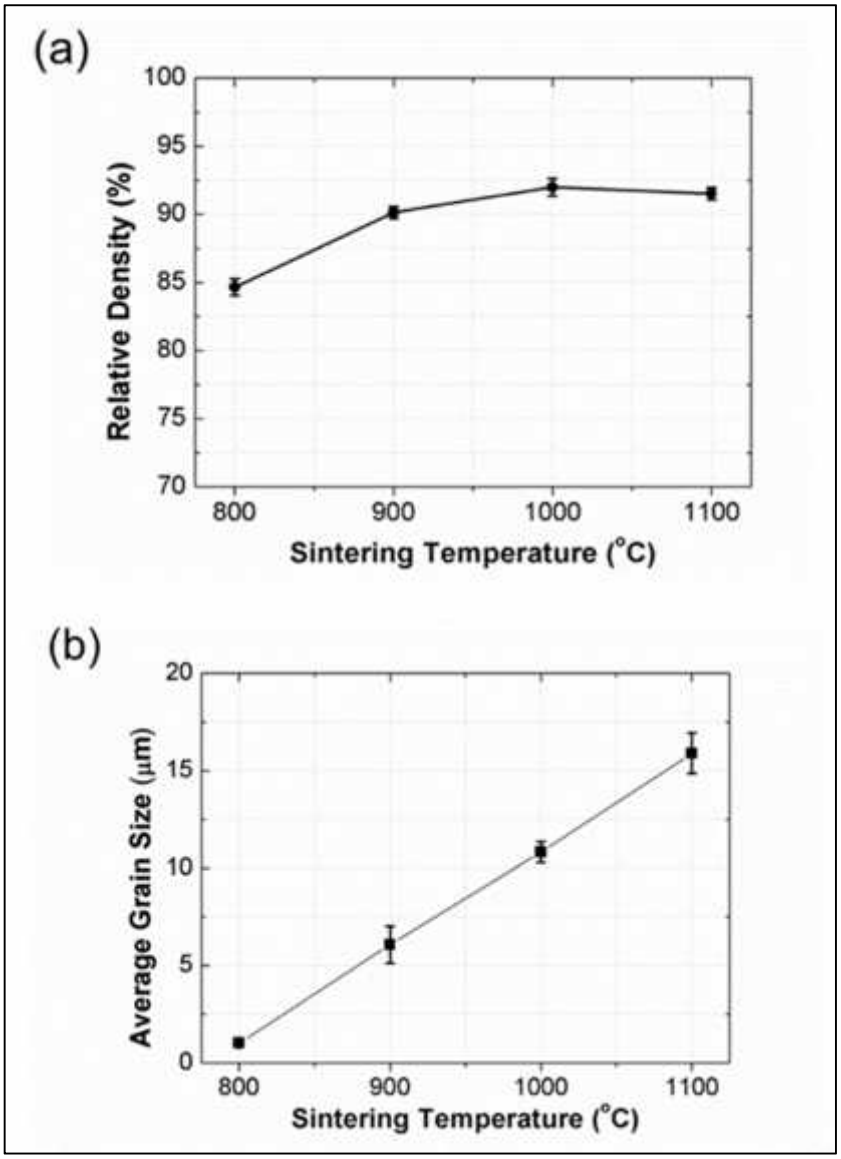

Figure 4.9: Effect of sintering temperature on a) the relative density and b) the average grain size of the yttria doped bismuth oxide ceramics.

The results of the systematic investigation of sintering/densification of YDB ceramics in this work were compared with reports in literature. Dordor et al. [35] reported a 84% relative density of 22.5YDB upon 48 hour sintering at 900 °C. On the other hand, with some isolated pores in the microstructure (similar to those shown in Figure 4.7b-d), Wang et al. [47] achieved 96% of the theoretical density for 24YDB ceramics upon 2 hours of sintering at 1025 °C. A similar density value was also reported by Joshi et al. [30] as a result of sintering 25YDB samples at 1000 °C for 12 hours. These results suggest similar densification rates reported in the present work.

In contrast to these results, Zhen et al. [40] achieved a relative density of 96% with an average grain size of ca. 100 nm in the sample that was prepared by reactive sintering at 600 °C for 2 hours.

4.3. Electrical Properties of YDB Ceramics

For YDB ceramics to be useful for SOFC applications, their ionic conductivity must be sufficient. Therefore, electrochemical impedance spectroscopy (EIS) measurements were performed on the YDB ceramics using Ag contacts to determine their electrical conductivity. The measured electrical conductivity results in EIS will be same as the ionic conductivity value since the transference number of YDB for the oxygen ion conductivity is unity in air [48].

The advantage of the EIS technique is that it distinguishes the electrolyte resistance from that of the contact. An example Nyquist plot obtained by the EIS measurements performed on the YDB ceramics sintered at 800 °C is given in Figure 4.10. The first intercept at the horizontal axis is named as the area specific resistance 1 (ASR1) and the distance between the first and the second intercepts of the semi-circle is named as the area specific resistance 2 (ASR2, Figure 4.10). The semi-circles in general suggest that there is a capacitive element parallel to the observed resistance, which usually points to an electrochemical process (e.g., oxygen adsorption/desorption, oxygen reduction and etc.) at Ag electrodes at this temperature. The oxygen ion conduction of bismuth oxide based ceramics in our measurement with the temperature range (350-650 °C) exhibits an ohmic (non-capacitive) behavior [49]. Therefore, the ASR1 is assigned to the resistance to the ion conduction within YDB, while ASR2 is ascribed to the oxygen reduction/evolution processes at the Ag electrode surface.

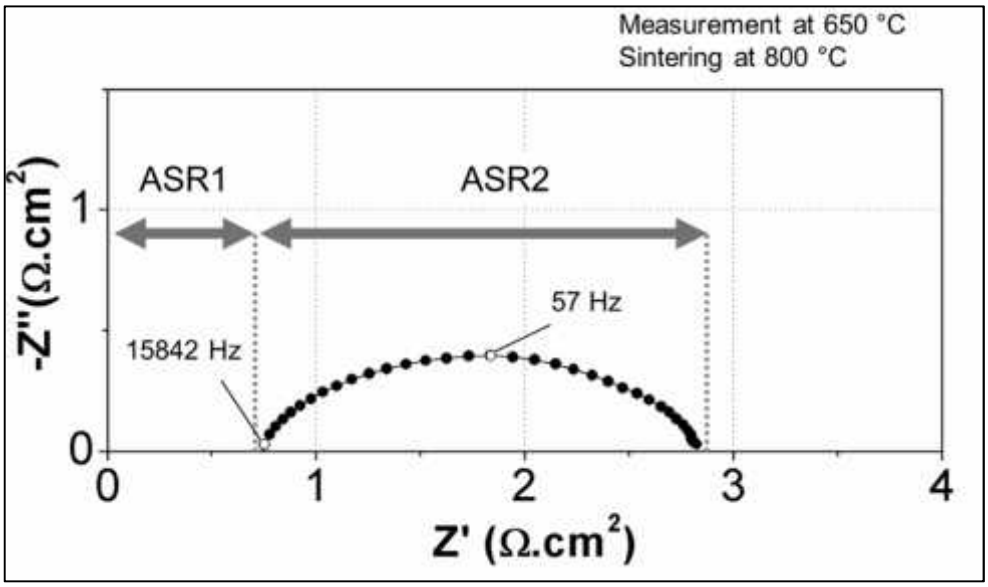

Figure 4.10: Representative Nyquist plot obtained at 650 °C from the symmetrical half-cell consisting of Ag electrodes and yttria doped bismuth oxide ceramic electrolyte sintered at 800 °C.

Figure 4.11 shows the Nyquist plots of the EIS data collected from YDB ceramics at 450, 550 and 650 °C. In all samples, ASR1 shifted to lower values, as expected from a thermally activated oxygen ion conduction. ASR2, earlier ascribed to oxygen reduction/evolution processes at the Ag electrodes also show a similar trend, consistent with a thermally activated electrochemical process. The only exception appears to be the transition from 450 to 550 °C in the YDB ceramic sintered at 800 °C (Figure 4.11a). This is considered to be due to the microstructural evolution of the Ag electrode fabricated from an in-house ink during the heating up process.

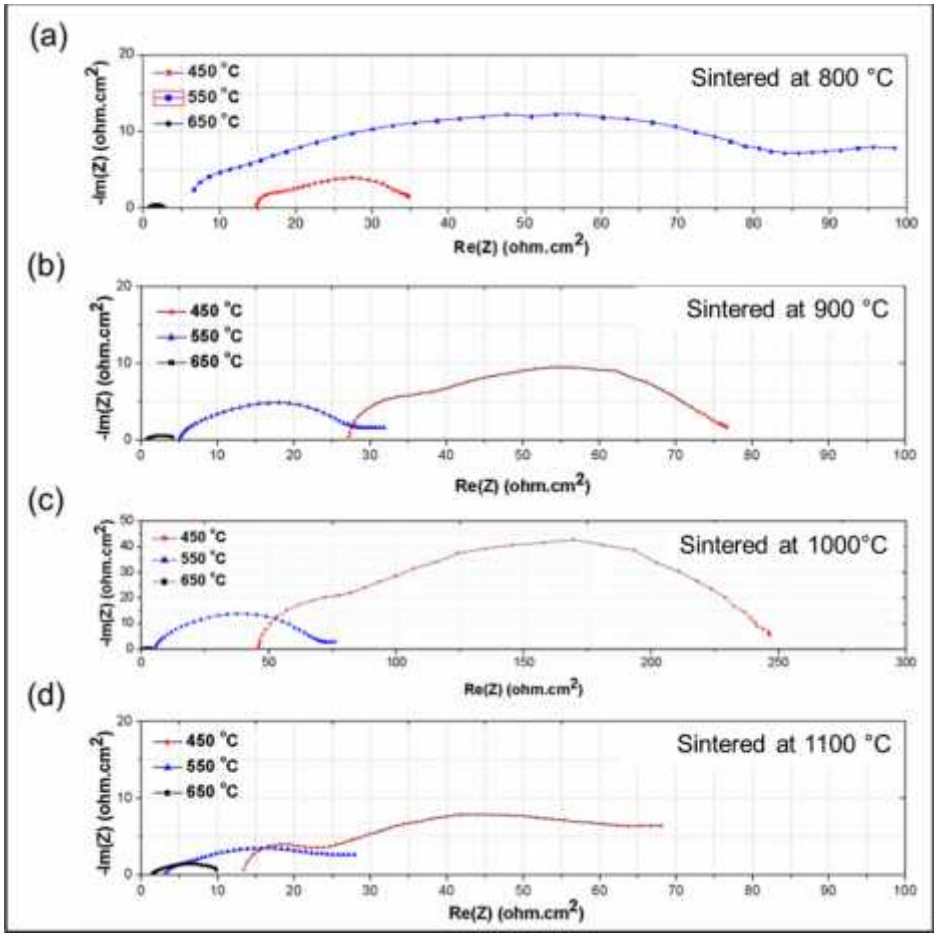

Figure 4.11. The Nyquist plot shows ASR values of 4 YDB samples sintered at 800-1100 °C.

From the ASR1 data collected at a wide range of temperatures (350-650 °C), the electrical conductivity values of the YDB ceramics were calculated using the following equation:

$$\sigma = \frac{T}{ASR1} \qquad (3.3),$$

where T is the thickness of electrolyte, i.e., the distance between electrodes.

The dependence of the electrical conductivity of the YDB ceramics on temperature is provided in Figure 4.12. YDB ceramic sintered at 800 °C, exhibits an Arrhenius-type of temperature dependence of conductivity with a single activation energy of 1.01 eV (± 0.03). This sample also exhibits slightly higher electrical conductivity than those sintered at higher temperatures, which is likely connected to its more open structure, evidenced by the larger lattice parameter (Table 4.1). Overall, similar conductivity values with Arrhenius type of temperature dependences are

observed in samples sintered at 900-1100 °C below 600 °C. An increase in conductivity in an irregular manner is apparent at higher temperatures (Figure 4.12). In the literature, a decrease in the slope of the Arrhenius graph of electrical conductivity has been reported for almost all rare-earth doped Bi_2O_3 ceramics [10], [31], [32], [50]. This phenomenon has been attributed to the order-disorder transition taking place at around 600 °C [10], [31], [33], [50]. However, to capture the slope decrease clearly, a new sample was used to avoid any structural changes that may take place during measurement [32]. The irregular nature of the conductivity increase observed above 600 °C in the present case (Figure 4.12) is possibly caused by such changes in the sample. Below 600 °C, activation energy values of 1.11 eV (± 0.02), 1.15 eV (± 0.02) and 1.07 eV (± 0.01) are calculated for YDB ceramics sintered at 900, 1000 and 1100 °C respectively; seen in Table 4.2. These values are in agreement with those reported for 25YDB by Tan et al. [45].

When the electrical conductivity values are compared, the highest conductivity value of 0.1 S/cm is observed for the YDB sintered at 800 °C. This observed conductivity value is identical to that reported in the literature, i.e., 0.11 , 0.07 and 0.18 S/cm were reported at 650 °C [51], 600 °C [44] and 700 °C [30] respectively. Even at lower annealing temperatures – 500 °C, Lee et al. [44] observed an ionic conductivity of 0.015 S/cm for YDB ceramic sintered at 800 °C which is similar to the conductivity value (0.011) observed in this study when the same sintering temperature is used (Figure 4.12).

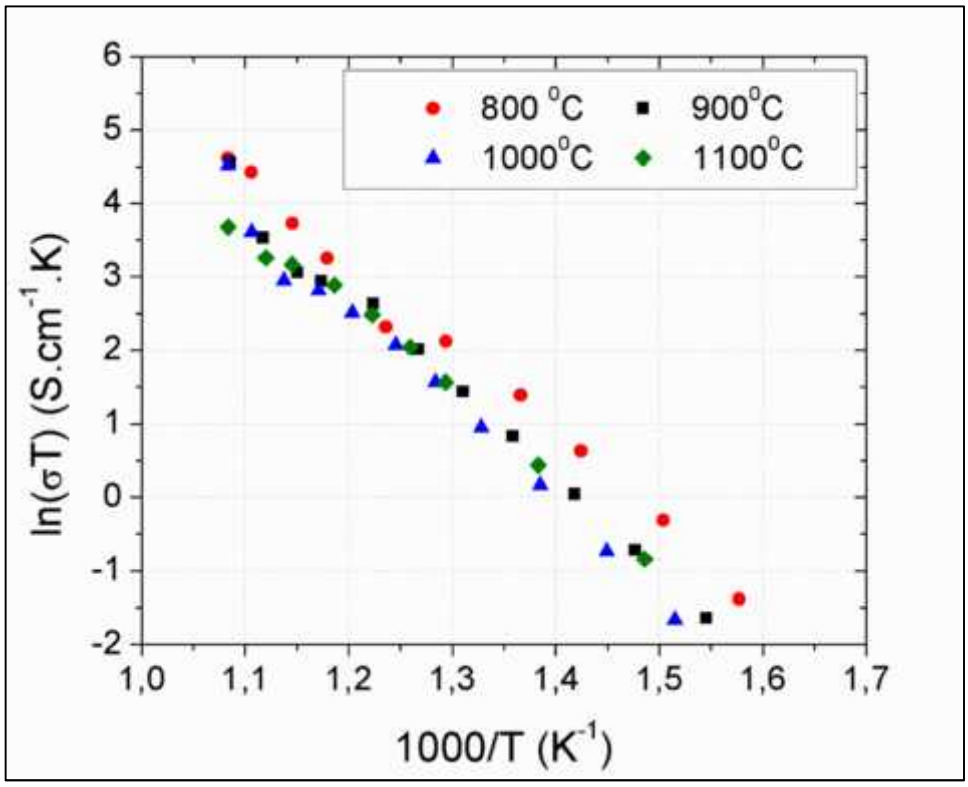

Figure 4.12. Temperature dependence of the electrical conductivity of yttria doped bismuth oxide ceramics sintered at 800, 900, 1000 and 1100 °C for 6 hours, in air.

Table 4.2. Activation energy values with error bars for YDB samples sintered at various sintering temperatures.

Tsintering	Ea (eV)	Error (eV)
800	1.01	0.03
900	1.11	0.02
1000	1.15	0.02
1100	1.07	0.01

4.4. Long-term Stability of YDB Ceramics

4.4.1. Background and Approach

Since the long-term stability of the high ionic conductivity of the bismuth oxide-based ceramics is crucial for their applicability in SOFCs, significant research focused on this issue [10], [30], [31], [33], [47]. Experiments have shown that the commonly used 25 mol% Y_2O_3 doped Bi_2O_3 (YDB) exhibits a fast decay in the ionic conductivity

with time upon prolonged exposure to 650 °C [10]. The same study has also shown that this conductivity decay is accompanied by a phase transformation from cubic-δ to rhombohedral [10]. The conductivity degradation due to this phase transformation has been supported by the investigations on the Bi_2O_3 - Y_2O_3 phase diagram, suggesting that the cubic-δ phase observed at ≤650 °C in many studies [10], [31]-[33], [52] are only metastable and that a 25 mol% Y_2O_3 doped Bi_2O_3 (25YDB) should eventually transform into a mixture of rhombohedral (denoted as I in Figure 4.13) and C-type cation-ordered cubic (denoted as II) structures (Figure 4.13) [41].

Many studies exist on the effect of the amount and type of dopants on the structural stability of bismuth oxide at 650 °C [30], [53], [54]. The effect of fabrication temperature, on the other hand, on the structural and electrical conductivity stability has not been studied yet. A gas-tight YDB ceramic with less than 10% porosity is required for SOFC and oxygen separation membrane applications and achievement of this density may be possible upon sintering at a wide range of temperatures, depending on the powder characteristics. For example, Joshi et al sintered 25YDB pellets at 1000 °C [30], while Zhen et al. was able to achieve ca. 95% relative density upon sintering 25YDB at 550-670 °C [40], both observing pure cubic-δ phase in their room-temperature X-ray diffraction studies. On the other hand, according to the phase diagram by Watanabe given in Figure 4.13 [41], the former fabrication condition corresponds to the phase stability region of pure cubic-δ, while the latter is in the rhombohedral + C-type cation ordered cubic two-phase region (denoted as I+II in Figure 4.13). Therefore, the cubic-δ phase observed by Zhen et al. is entirely metastable [40], while that reported by Joshi et al [30] is entirely stable.

In the present work, we investigate the effects of sintering temperature on the phase and electrical conductivity stability of Y_2O_3 doped Bi_2O_3, for the first time in the literature. The Y_2O_3 doping amount is selected as 28 mol%, while the sintering is carried out at 800, 900, 1000 and 1100 °C to ensure that i) the powder compacts can be sintered to acceptable density, and more importantly ii) three different phase stability regions in the Watanabe's phase diagram are covered, as marked by red circles in Figure 4.13 [41].

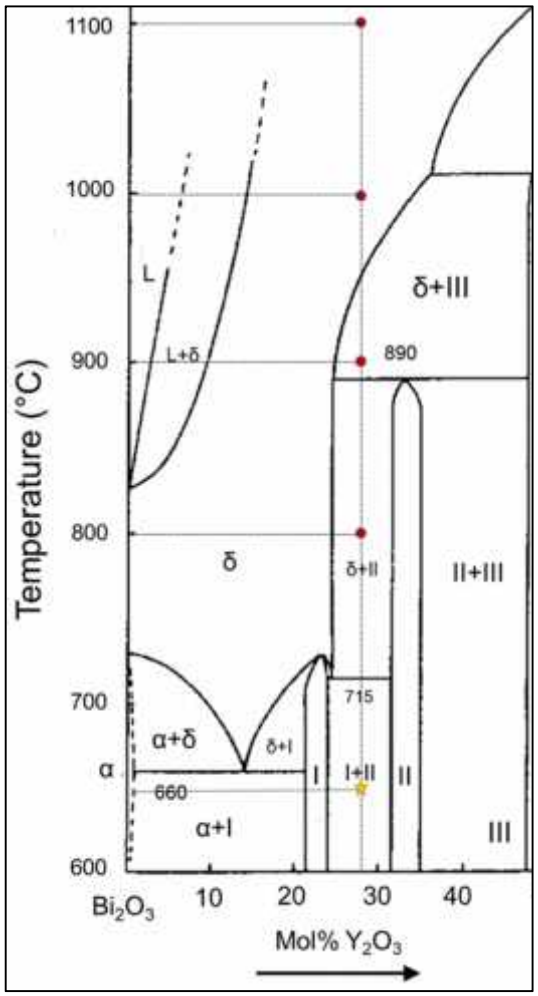

Figure 4.13: A phase diagram shows stable and metastable phase regions for YDB components.

Table 4.3: A collected data according to phase diagram of Watanabe.

$T_{sintering}$ (°C)	Observed Phases after Sintering (mol%)	Stable Phases at $T_{sintering}$ (mol%)	Metastable Phases (mol%)	Stable Phases at the Operating Temperature of 650 °C (mol%)
800	fcc-δ (100%)	fcc-δ (50%) + Cation-ordered cubic (50%)	fcc-δ (50%)	Rhombohedral (46%) + Cation-ordered cubic (54%)
900	fcc-δ (100%)	fcc-δ (88%) + Triclinic (12%)	fcc-δ (12%)	
1000	fcc-δ (100%)	fcc-δ (100%)	0%	
1100	fcc-δ (100%)	fcc-δ (100%)	0%	

4.4.2. Effect of Sintering Temperature on The Long-Term Stability of YDB Ceramics

It is desirable that the relatively high electrical conductivity of YDB ceramics is maintained upon long-term operation. Although studies in this matter have previously been carried out in the literature [10], [30]-[33], the effect of sintering temperature on the longevity of the electrical conductivity of YDB ceramics has not been investigated yet. Figure 4.14 shows the dependence of the normalized electrical conductivity values on the time the YDB ceramics sintered at 800-1100 °C are exposed to 650 °C, in stagnant air. The conductivity of the YDB ceramics sintered at 900, 1000 and 1100 °C increases slightly in the first 10 hours, but then decreases linearly in the remaining 90 hours of the experiment (Figure 4.14). Interestingly, the YDB ceramic sintered at 800 °C exhibits a much faster, exponential-type decay in the normalized electrical conductivity (Figure 4.14). This suggests that the conductivity decay takes place via the same mechanisms in YDB ceramics sintered at 900, 1000 and 1100 °C, while in the YDB sintered at 800 °C, a different mechanism governs the conductivity decay.

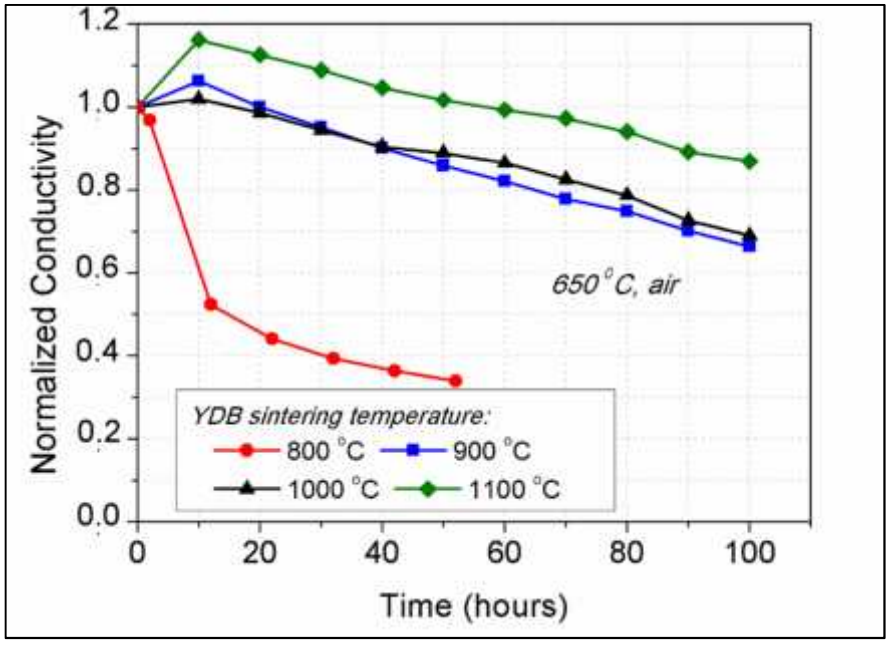

Figure 4.14. Changes in the electrical conductivities of the yttria doped bismuth oxide ceramics sintered at 800, 900, 1000 and 1100 °C with time upon prolonged exposure to stagnant air, at 650 °C.

In order to determine whether the conductivity decay is related to any phase transformations, XRD analyses were performed on the YDB samples sintered at these

four temperatures after exposure to 650 °C for 100 hours (Figure 4.15). Evidently, the fluorite structure is retained in all samples but the one sintered at 800 °C, which exhibits diffraction peaks belonging to the rhombohedral phase (Figure 4.15). From the intensities of the most intense peaks of the cubic and rhombohedral phases, the amount of the rhombohedral phase is roughly calculated as 16 mol%. The sample that exhibits a different (faster) conductivity decay kinetics is the only one that undergoes phase transformation from cubic to rhombohedral. On the other hand, since the stable phases are rhombohedral and C-type ordered cubic at the operating temperature of 650 °C (Figure 4.13), it is reasonable to expect that eventually all samples will consist of a mixture of these two phases. A freshly prepared batch of YDB ceramics were subjected to 300 hours of annealing at 650 °C and their XRD analyses were performed to determine whether any secondary phase formation takes place in the samples sintered at temperatures higher than 800 °C. Evidently, still solely δ-cubic phase is present in the YDB samples sintered at 1000 and 1100 °C (Figure 4.16). The main rhombohedral phase peak is now only barely detectable in the YDB sintered at 900 °C (Figure 4.16-inset), while the amount of the rhombohedral phase increased from 16 to 25 mol% in the YDB sintered at 800 °C (Figure 4.16).

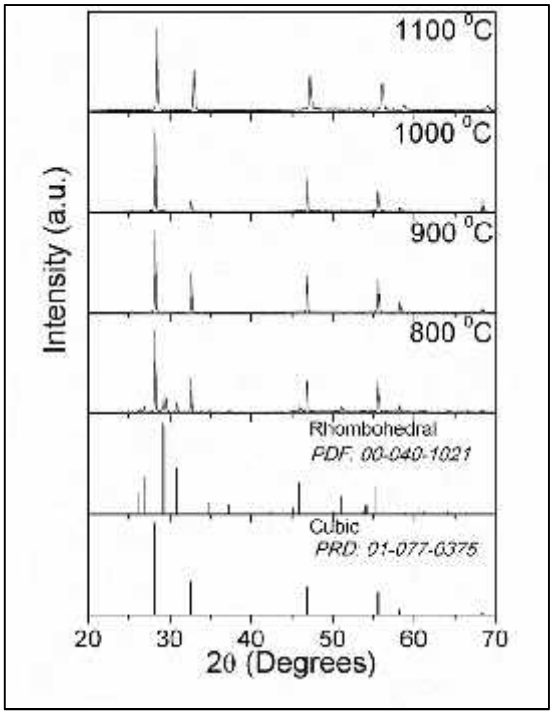

Figure 4.15: X-ray diffraction patterns obtained from the yttria doped bismuth oxide ceramics sintered at 800, 900, 1000 and 1100 °C for 100 hours after prolonged exposure to stagnant air, at 650 °C.

Interestingly, even after 300 hours, the only YDB ceramic that undergoes significant phase transformation from cubic to rhombohedral, YDB sintered at 800 °C, is the one that has a significant amount of metastable cubic-δ phase in the as-sintered state (50 mol%, Table 4.3). This sample is also the one with the highest lattice parameter (Table 4.1), which we attribute to the dominance of $Y_i^{\cdots}$ formation over Y_{Bi}^{x} (Equations 3.1 and 3.2). Fung et al. proposed that the phase transformation in YDB ceramics takes place via a nucleation and growth mechanism and its rate is controlled by the cation diffusion [54]. In the present case, it is proposed that the cation diffusion (and hence the cubic to rhombohedral phase transformation) is facilitated by the formation of $Y_i^{\cdots}$ and $V_{Bi}^{'''}$ defects that exist in higher amounts in the YDB sintered at 800 °C. This also suggests that the preference of the Y^{3+} of the interstitials rather than the regular Bi^{3+} sites occurs predominantly in the metastable cubic-δ phase of the YDB ceramics. This argument is supported by the appearance of a small rhombohedral peak after 300 hours at 650 °C in the YDB sintered at 900 °C, which contains ca. 12 mol% metastable cubic-δ phase (Table 4.3) and has the second highest lattice parameter. On the other hand, the conductivity decay in the YDB sintered at 900 °C in the first 100 hours of exposure to 650 °C is not concomitant with cubic to rhombohedral phase transformation since i) no trace of rhombohedral phase formation is observed in the XRD data collected after 100 hours of annealing at 650 °C (Figure 4.15) and ii) the conductivity decay kinetics of YDB sintered at 900 °C resembles that of YDB ceramics sintered at 1000 and 1100 °C, which remain cubic even after 300 hours of annealing at 650 °C (Figure 4.14). Therefore, the conductivity decay observed in the samples sintered at 900, 1000 and 1100 °C must be occurring via the same mechanism.

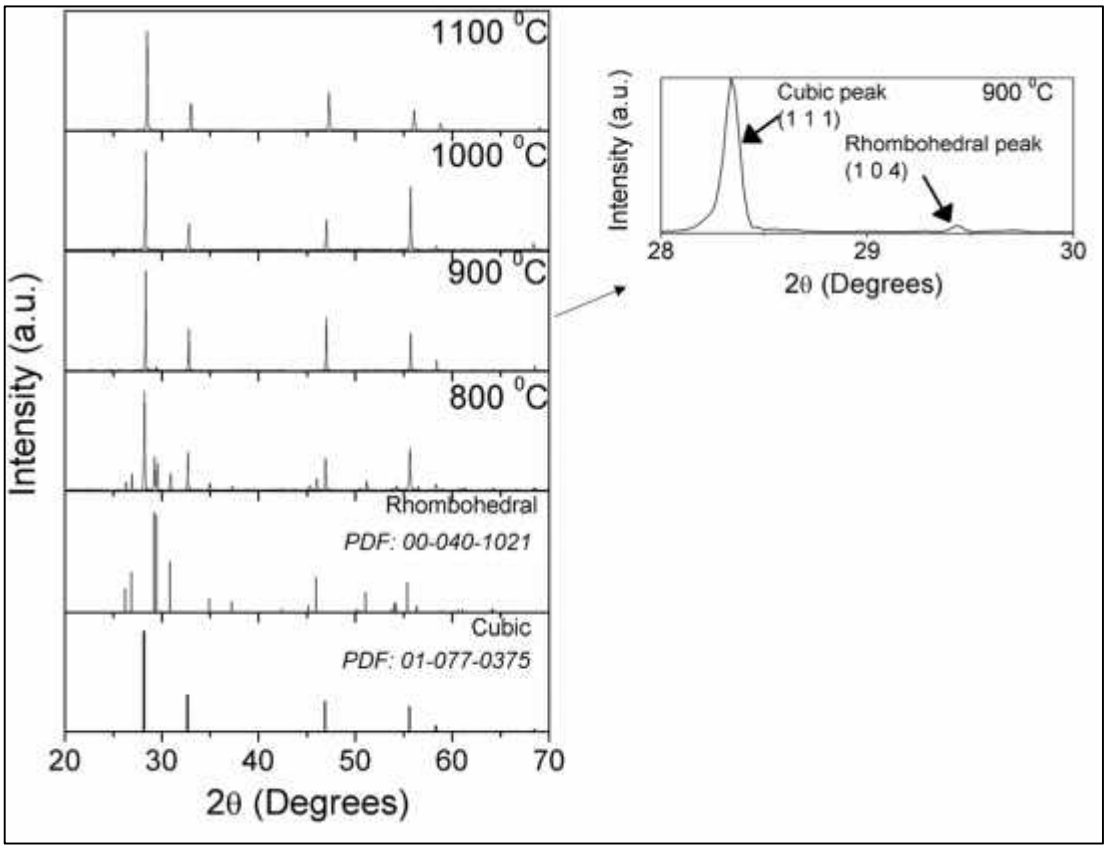

Figure 4.16: X-ray diffraction patterns obtained from the yttria doped bismuth oxide ceramics sintered at 800, 900, 1000 and 1100 °C for 300 hours after prolonged exposure to stagnant air, at 650 °C.

However, crystal structure change in some of YDB samples was shown via XRD above, microstructural investigation of those samples needs to be performed via SEM. The samples sintered at 800-1100 °C analysized via SEM after 100 and 300 hours longevity test at 650 °C as shown in Figure 4.17. Platelet type morphology indicative of the presence of the rhombohedral phase (as evidenced by the XRD analysis in Figure 4.16-4.17) was observed in YDB ceramics sintered at 800 °C (Figure 4.17a) and platelet like structure expand all the structure after 300 hours annealing (Figure 4.17e). However, the structure of the sample sintered at 900 °C did not show any phase transformation between as-sintered (Figure 3.7b) and 100 hours annealed (Figure 4.17b) state, a platelet like structure evidence started to be seen after 300 hours longevity test (Figure 4.17f).

On the other hand, the as-sintered microstructures of the YDB ceramics sintered at 1000-1100 °C (Figure 4.7) remains unchanged (Figure 4.17cdgh).

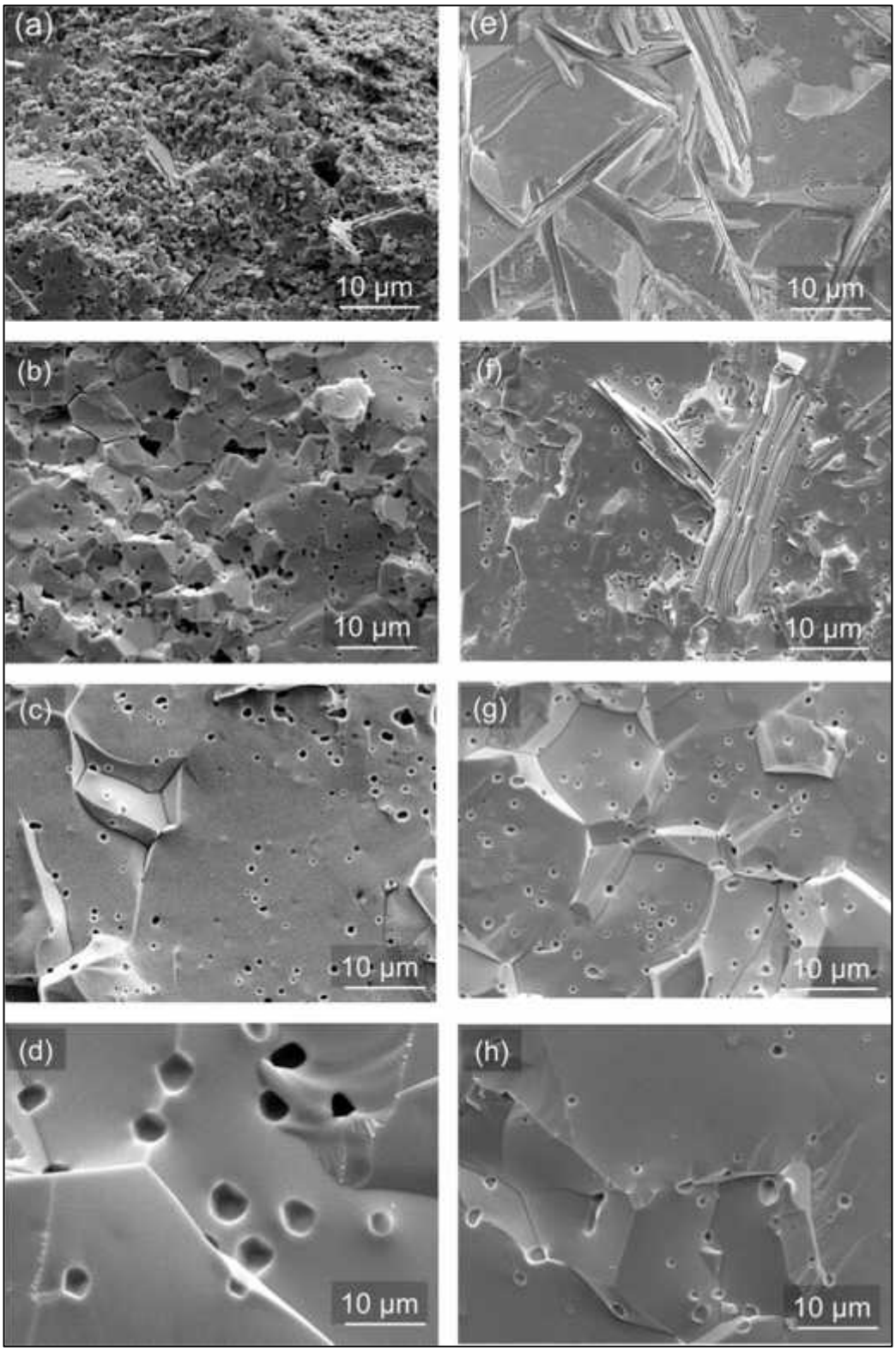

Figure 4.17: Scanning electron microscopy images of the fracture surfaces of the yttria doped bismuth oxide ceramics sintered at a and e) 800, b and f) 900, c and g) 1000, d and h) 1100 °C for 100 hours (a-d) and 300 hours (e-f) after prolonged exposure to stagnant air at 650 °C.

In the literature, two sources of electrical conductivity loss in bismuth oxide-based ceramics upon long-term operation have been mentioned [10], [28], [31], [33]. The ordering of the oxygen sublattice is one of the sources and it does not induce any changes in the XRD patterns [10], [28], [33]. Although this phenomenon resembles the present case of YDB ceramics sintered at 900-1100 °C, the fact that anion ordering that takes place upon long-term operation at temperatures below 600 °C and that the conductivity decay is much faster than that observed here in Figure 4.14 [10], [28], [33] rules this possibility out. Another source of conductivity decay reported in the literature is the transformation of the δ-phase into a rhombohedral structure with lower ionic conductivity [10], [31], [33]. This type of degradation is reported to take place at 650 °C [10], [31], [33] and is in agreement with the XRD data (Figure 4.15-4.16) and the platelet-type particles observed in the SEM images (Figure 4.17aef) indicating the formation of rhombohedral phase under the same experimental conditions in the YDB ceramic prepared by sintering at 850 °C. It should be noted that a different type of conductivity decay kinetics is seen in the YDB ceramics sintered at 900-1100 °C with no signs of phase transformations except 900 °C with the little amount of platelet-type structure occurs after 300 hours annealing, despite being subjected to the same long-term stability testing conditions (Figure 4.15, 4.16, 4.17).

Here, for the interpretation of the effect of sintering temperature on the longevity of the electrical conductivity of YDB ceramics, we revisit the phase diagrams proposed by Datta and Meehan [29] and Watanabe [41]. The former asserts that the δ-phase should be stabilized by 28 mol% Y_2O_3 addition at temperatures higher than 500 °C [29]. On the other hand, Watanabe suggests that the cubic δ-phase observed in similar compositions at temperatures below 940 °C is only metastable and upon long-term exposure to these temperatures, transformations into the stable phases will take place eventually [41]. This means that the cubic δ-phases observed here upon sintering at 800 and 900 °C are in part metastable, while cubic δ-phase observed upon sintering at 1000 and 1100 °C are completely stable. In fact, upon a detailed examination of the phase diagram by Watanabe [41], upon sintering at 900 °C, only a small amount (12 mol%) of triclinic phase should be stable along with a majority of (88 mol%) cubic δ-phase (Table 4.3). On the other hand, the stable phase composition of the YDB ceramics should lie at a 1:1 mixture of cubic δ and cation-ordered cubic phases (Table 4.3). Assuming that any amount of cubic δ-phase that, in fact would be replaced by another phase upon long-term heat treatment at the given sintering temperatures would

be metastable, it can be deduced that the YDB ceramics sintered at 800 and 900 °C contain respectively 50 and 12 mol% metastable cubic δ-phase (Table 4.3).

According to the data given in Table 4.3 [41], upon long-term operation at 650 °C, the YDB ceramics sintered at 1000 and 1100 °C should both undergo phase transformations from a 100 mol% stable cubic δ into a mixture of rhombohedral (46 mol%) + cation-ordered cubic (54 mol%). Hence, a similar conductivity decay kinetics (as seen in Figure 4.14) corresponding to a similar phase transformation kinetics may be expected. The YDB ceramic sintered at 900 °C also consists mainly of a stable cubic δ phase (88 mol%), therefore a phase transformation kinetics (hence a conductivity decay kinetics, Figure 4.14 similar to that observed in YDB ceramics sintered at 1000 and 1100 °C is logical. The fact that no phase transformation is observable in the XRD patterns of YDB ceramics sintered at 900-1100 °C may be due to the small amounts of newly formed phases that are not detectable by XRD at this point.

Differential thermal analysis (DTA) has been used in the literature on bismuth oxide based materials to determine whether any phase transformations or ordering has taken place upon long-term operation. For example, Kruidhof et al. attributed the endothermic peak observed at 748 °C when a YDB ceramic with the rhombohedral structure was heated up to the rhombohedral to cubic phase transformation [31]. On the other hand, the endothermic peak observed by Jiang et al [33] at 630 °C was attributed to the order-disorder transition taking place in a YDB ceramic that had been exposed to 500 °C for 500 hours. In the present study, we performed DTA analyses on YDB ceramics exposed to 650 °C for 300 hours (Figure 4.18). Evidently, the YDB sintered at 800 °C exhibits an endothermic peak at 746 °C, which indicates the transformation of the rhombohedral phase observed in Figures 4.15 and 4.16 to δ-cubic. This result is in agreement with that reported by Kruoidhof et al. [31] and suggests that no detectable phase transformations take place in the YDB ceramics sintered at 900-1100 °C in the present study.

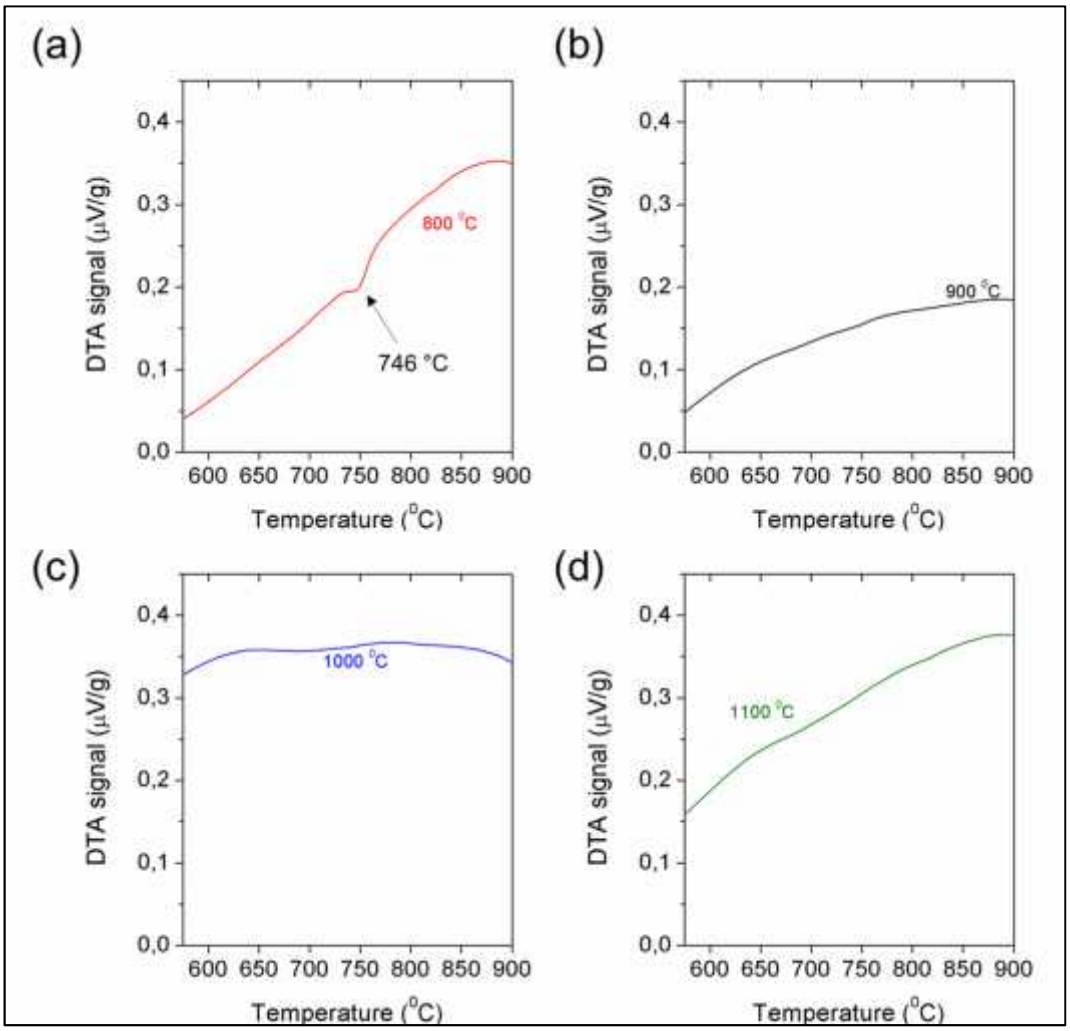

Figure 4.18: The DTA analysis of the sintered YDB samples at 800-1100 °C refered as a to d, respectively; after annealing at 650 °C for 300 hours.

5. CONCLUSION

The aim of the work was to fabricate the fast ion conductor yttria doped bismuth oxide (YDB) and investigate the effects of the fabrication conditions on its long-term stability at the relevant solid oxide fuel cell (SOFC) operating temperatures (i.e., 650 °C). For this purpose, YDB powders synthesized by a Pechini method was consolidated and sintered at 800-1100 °C. Relative densities exceeding 90% with no interconnected porosity was achieved.

The electrical conductivity of the YDB ceramics were determined via electrochemical impedance spectroscopy, which allowed the separation of the resistance to the ion conduction within the YDB ceramic from that of the contact. The determined ionic conductivity values of ca. 0.1 S/cm at 650 °C were in the range of those reported in the literature. The long-term stability of the electrical conductivity revealed that upon prolonged exposure to 650 °C, YDB ceramics sintered at 800 °C exhibited an exponential-type of conductivity decay, while a slower, linear-type of conductivity decay took place in samples sintered at 900, 1000 and 1100 °C. Post-mortem characterization of the YDB samples subjected to long-term testing was carried out by X-ray diffraction (XRD) and scanning electron microscopy (SEM) analyses to determine the causes of the difference in the conductivity decay characteristics. XRD analyses revealed that even after 300 hours of exposure to 650 °C, only the YDB sintered at 800 °C had significant amounts of rhombohedral phase transformed from the high conductivity cubic-δ phase. Confirming this finding, SEM images showed significant amounts of platelet-type of grains within the microstructure of the sample sintered at 800 °C.

The relative stability of the YDB ceramics sintered at 900, 1000 and 1100 °C was connected to the premise that they contain either no or smaller amounts of metastable cubic-δ phase in their as-sintered state, in accordance with the phase diagram by Watanabe [41]. The YDB ceramic sintered at 800 °C, also the sample with the highest amount of metastable cubic-δ phase, had the largest lattice parameter suggesting that of $Y_i^{\cdot\cdot\cdot}$ and $V_{Bi}^{'''}$ were predominantly present. The presence of these defects were connected to more facile cation diffusion and thus faster cubic to rhombohedral transformation in the YDB sintered at 800 °C.

From a practical point of view, for SOFC applications it is preferable that the YDB ceramics are sintered at temperatures which no metastable cubic-δ phase would be present, i.e., 900-1100 °C. These temperatures also ensure relative densities higher than 90%.

REFERENCES

[1] Barbir F., Veziroğlu T.N., Plass Jr.H.J., (1990), "Environmental damage due to fossil fuels use", International Journal of Hydrogen Energy, 15, 739-749.

[2] Halinen M., (2015), "Improving The Performance Of Solid Oxide Fuel Cell Systems", Doctoral Thesis, Aalto University School of Science.

[3] Singhal S.C., Kendall K., (2003), "High temperature solid oxide fuel cells: fundamentals", Design and Applications, ISBN 1856173879, Elsevier Advanced Technology.

[4] Baharuddin N. A., Muchtar A., Somalu M.R., Anwar M., H. M.A.S.A.K.A., Mah J., (2018), "Effects of sintering temperature on the structural and electrochemical properties of $SrFe_{0.5}Ti_{0.5}O_3$-δ perovskite cathode", International Journal of Applied Ceramic Technology, 15, 338–348.

[5] Sillen L. G., (1937), "X-ray studies on bismuth trioxide", Arkiv for Kemi, Mineralogi och Geologi, 12A, 1-15.

[6] Azad A.M., Larose S., Akbar S.A., (1994), "Bismuth oxide-based solid, electrolytes for fuel cells", Journal of Materials Science, 29, 4135-4151.

[7] Wachsman E.D., 2004, "Effect of oxygen sublattice order on conductivty in highly defective fluorite oxides", Journal of European Ceramics Society, 24, 1281-1285.

[8] Boyapati S., Wachsman E.D., Jiang A., (2001), "Effect of oxygen sublattice ordering on interstitial transport mechanism and conductivty activation energies in phase-stabilized cubic bismuth oxides", Solid State Ionics, 140, 149-160.

[9] Jiang N., Wachsman E.D., (1999), "Structural stability and conductivty of phase-stabilized cubic bismuth oxides", Journal of the American Ceramic Society, 82, 3057-64.

[10] Jiang N., Buchanan R.M., Henn F.E.G., Marshall A.F. and Stevenson D.A., Wachsman E.D., (1994), "Aging phenomenon of stabilized bismuth oxide, Materials Research Bulletin", 29, 247-254.

[11] Ostergard Ö.J.L., Clausen C., Bagger C., Mogensen M., (1995), "Manganite-zirconia composite cathodes for SOFC: influence of structure and composition", Electrochimica Acta, 40, 1971-1981.

[12] Murray E.P., Tsai T., Barnett S.A., (1998), "Oxygen transfer processes in $(La,Sr)MnO_3/Y_2O_3$-stabilized ZrO_2 cathodes: an impedance spectroscopy study", Solid State Ionics, 110, 235-243.

[13] Wilson J.R., Barnett S.A., (2008), “Solid oxide fuel cell Ni–YSZ anodes: effect of composition on microstructure and performance”, Electrochemical and Solid-State Letters, 11, B181-B185.

[14] Zhu W.Z., Deevi S.C., (2003), “A review on the status of anode materials for solid oxide fuel cells”, Materials Science and Engineering: A, 362, 228-239.

[15] Gentile P.S., (2007), “Development of A Novel High-Performance Electrolyte Supported Solid Oxide Fuel Cell”, Master’s Thesis, Montana State University.

[16] Wachsman E.D., Lee K.T., (2011), “Lowering the temperature of solid oxide fuel cells”, 334, 935-939.

[17] Chen Y., Jung W., Cai Z., Kim J.J., Tuller H.L., Yildiz B., (2012), “Impact of Sr segregation on the electronic structure and oxygen reduction activity of $SrTi_{1-X}Fe_xO_3$ surfaces”, Energy Environmental Science, 5, 7979-7988.

[18] Chen H.Y., Yu H.C., Cronin J.S., Wilson J.R., Barnett S.A., Thornton K., (2011), “Simulation of coarsening in three-phase solid oxide fuel cell anodes”, Journal of Power Sources, 196, 1333-1337.

[19] Sahibzada M., Steele B.C.H., Hellgardt K., Barth D., Effendi A., Mantzavinos D., Metcalfe I.S., (2000),” Intermediate temperature solid oxide fuel cells operated with methanol fuels”, Chemical Engineering Science, 55, 3077–3083.

[20] Sarantaridis, D., Atkinson, A., (2007), “Redox cycling of ni-based solid oxide fuel cell anodes: a review”, Fuel Cells, 7, 246–258.

[21] Cassidy M., Lindsay G., Kendal K., (1996), “The reduction of nickel-zirconia cermet anodes and the effects on supported thin electrolytes”, Journal of Power Sources, 61, 189-192.

[22] Faes A., Hessler-Wyser A., Presvytes D, Vayenas C.G., Herle J.V., (2009), “Nickel–zirconia anode degradation and triple phase boundary quantification from microstructural analysis”, Fuel Cells, 9, 841-851.

[23] Sammes N.M., Tompsett G.A., Nafe H., Aldinger F., (1999), “Bismuth based oxide electrolytes – structure and ionic conductivity”, Journal of European Ceramic Society, 19, 1801-1826.

[24] Fung K.Z., Baek H.D., Virkar A.V., (1992), “Thermodynamic and kinetic considerations for Bi_2O_3-based electrolytes”, Solid State Ionics, 52, 199-211.

[25] Mairesse G., (1993), “Bismuth-based oxide conductors novel structural and electrical features”, Fast Ion Transport in Solids, 250, 271-290.

[26] Kruidhof H., (1990), Thermochemical stability and nonstoichiometry of yttria-stabilized bismuth oxide solid solutions”, Solid State Ionics., 37, 213–215.

[27] Takahashi T., Esaka T., Iwahara H., (1975), “High oxide ion conduction in the sintered oxides of the system Bi_2O_3-Gd_2O_3”, Journal of Applied Electrochemistry, 5, 197–202.

[28] Kruidhof H., Bouwmeester H., Devries K., Gellings P., Burggraaf A., (1992, “Thermochemical stability and nonstoichiometry of erbia-stabilized bismuth oxide”, Solid State Ionics, 50, 181–186.

[29] Datta R.K., Meehan J.P., (1971), “The system Bi_2O_3-R_2O_3 (R=Y, Gd), Zeitschrift für anorganische und allgemeine Chemie, 383, 328–337.

[30] Joshi A.V., Kulkarni S., Nachlas J., Diamond J., Weber N., Virkar A.V., (1990), “Phase stability and oxygen transport characteristics of yttria- and niobia-stabilized bismuth oxide”, Journal of Materials Science, 25, 1237-1245.

[31] Boyapati S., Wachsman E.D., Jiang N., (2001), “Effect of oxygen sublattice ordering on interstitial transport mechanism and conductivity activation energies in phase-stabilized cubic bismuth oxides”, Solid State Ionics, 140, 149–160.

[32] Jung D.W., Duncan K.L., Camaratta M.A., Lee K.T., Nino J.C., Wachsman E.D., (2010), “Effect of Annealing Temperature and Dopant Concentration on the Conductivity Behavior in $(DyO_{1.5})_x$–$(WO_3)_y$–$(BiO_{1.5})_{1-x-y}$”, Journal of the American Ceramic Society, 93, 1384–1391.

[33] Jiang N., Wachsman E.D., (1999), “Structural stability and conductivity of phase-stabilized cubic bismuth oxides, Journal of the American Ceramic Society, 82, 3057-3064.

[34] Fung K.Z., Virkar A.V., (1991), “Phase stability, phase transformation kinetics, and conductivity of Y_2O_3—Bi_2O_3 solid electrolytes containing aliovalent dopants”, Journal of the American Ceramic Society, 74, 1970-1980.

[35] Dordor P.J., Tanaka J. and Watanabe A., (1987), “Electrical characterization of phase transition in yttrium doped bismuth oxide”, $Bi_{1.55}Y_{0.45}O_3$, Solid State Ionics, 25, 177-181.

[36] Jiang N., Buchanan R.M., Stevenson D.A., Nix W.D., Li J-Z., Yang J-L., (1995), “Anion ordering in aged stabilized bismuth oxide”, Materials Letters, 22, 215-219.

[37] Kruidhof H., Vries K.J.D., Burggraaf A.J., (1990), “Thermochemical stability and nonstoichiometry of yttria stabilized bismuth oxide solid solutions”, Solid State Ionics, 37, 213-215.

[38] Virkar A.V., Su P., Fung K-Z., (2002), “Massive transformation in bismuth oxide-based ceramics”, Metallurgical and Materials Transactions A, 33A, 2433-2443.

[39] Ekhelikar S., Bichile G.K., (2004), “Synthesis and structural characterization”, Bulletin of Material Science, 27, 19-22.

[40] Zhen Q., Kale G.M., Shi G., Li R., He W., Liu J., (2005), "Processing of dense nanocrystalline Bi_2O_3-Y_2O_3 solid electrolyte", Solid State Ionics, 176, 2727-2733.

[41] [41] Watanabe A., (1996), "Phase equilibria in the system Bi_2O_3-Y_2O_3: no possibility of δ-Bi_2O_3 stabilization", Solid State Ionics, 86-88, 1427-1430.

[42] Danks A.E., Hall S.R., and Schnepp Z., (2016), "The evolution of 'sol-gel' chemistry as a technique for materials synthesis", Royal Society of Chemistry, Materials Horizons, 3, 91.

[43] Zhang Y., Yang H., Li M., Sun B., Qi Y., (2010), "Improvement of multiple oxide properties: effect of gel processes on the quality of $Bi_2Sr_2CaCu_2O_8$ + δ superconducting powders", CrystEngComm, 12, 3046-3051.

[44] Lee J.G., Kim S.H., Yoon H.H., (2011), "Synthesis of yttria-doped bismuth oxide powder by carbonate coprecipitation for IT-SOFC electrolyte", Journal of Nanoscience and Nanotechnology, 11, 820-823.

[45] Tan M.Y., Tan K.B., Zainal Z., Khaw C.C., Chen S.K., (2012), "Subsolidus formation and impedance spectroscopy studies of materials in the $(Bi_2O_3)_{1-x}$ $(Y_2O_3)_x$ binary system", Ceramics International, 38, 3403-3409.

[46] Shannon R.D., (1976), "Revised effective ionic radii and systematic studies of interatomic distances in halides and chalcogenides", Acta Crystallographica A, 32, 751–767.

[47] Wang S.-F., Hsu Y.-F., Tsai W.-C., Lu H.-C., (2012), "The phase stability and electrical conductivity of Bi_2O_3 ceramics stabilized by Co-dopants", Journal of Power Sources. 218, 106–112.

[48] Singhal S.C., (2000), "Advances in solid oxide fuel cell technology", Solid State Ionics, 135, 305-313

[49] Li R., Zhen Q., Drache M., Rubbens A., Estournes C., Vannier R.-N., (2011), "Synthesis and ion conductivity of $(Bi_2O_3)_{0.75}(Dy_2O_3)_{0.25}$ ceramics with grain sizes from the nano to the micro scale", Solid State Ionics, 198, 6–15.

[50] Wachsman E.D., (2004), "Effect of oxygen sublattice order on conductivity in highly defective fluorite oxides", Journal of the European Ceramic Society, 24, 1281–1285.

[51] Shuk P., Wiemhofer H.-D., Guth U., Gopel W., Greenblatt M., (1996), "Oxide ion conducting solid electrolytes based on B_2O_3", Solid State Ionics, 89, 179-196.

[52] Zeng Y., Lin Y.S., (1999), "Stability and surface catalytic properties of fluorite-structured yttria-doped bismuth oxide under reducing environment", Journal of Catalysis, 182, 30–36.

[53] Fung K.Z., Chen J., Virkar A.V., (1993), “Effect of aliovalent dopants on the kinetics of phase transformation and ordering in RE_2O_3-Bi_2O_3 (RE = Yb, Er, Y, or Dy) solid solutions”, Journal of the American Ceramic Society, 76, 2403–2418.

[54] Fung K.Z, Virkar A.V., Drobeck D.L., (1994), “Massive transformation in the Y_2O_3-Bi_2O_3 system”, Journal of the American Ceramic Society, 77, 1638–1648.

BIOGRAPHY

I was born and raised in Bursa until university life begun at Gebze Technical University in Kocaeli. The reason I chose Materials Science and Engineering is due to my huge interest to science in general. I have completed English proficiency class in the first year of my university life, then started to attend lectures at Materials Science and Engineering department. In the first year at MSE department, I joined at the GTU rowing team of my university. In the second year at MSE department, I became an editor-in-chief of the first student magazine of this university which was my dream to prepare and publish during the university life since secondary school. Following summer of the year in 2014, I participated a volunteering organization – Aiesec, went to Tunisia for 7 weeks due to a journalism internship. In third year, I passed the ERASMUS+ exam for becoming an exchange student then I have done my mandatory internships in TUBITAK MAM and GTU Piezoelectric Lab.. The following year, I had been to Poland as an exchange student at Silesian Technology of University for 5 months. After coming back to Turkey, I have completed my BSc. with the graduation project ‘’Synthesizes of bismuth oxide nanoparticles and their fabrication into dense, thin ceramic sheets for low temperature solid oxide fuel cell applications’’ given by Dr. Aligul Buyukaksoy. Without wasting time, I immediately enrolled Department of Materials Science and Engineering at TR. Gebze Tehnical University Graduate School of Natural and Applied Sciences to continue the bachelor thesis in order to develop the project and myself with gaining more hands-on experience. I have completed my lectures in 2 terms at MSc and was accepted by a researcher named Dr. Soren from Denmark Technical University by ERASMUS+ Traineeship program for 2 months. After I have completed all my tasks and have written up a report comfortably, a massive work started with more focusing on the MSc thesis in Turkey. Currently I am a scholar in a TUBITAK project (217M031) and have worked on the same study within this thesis.